

1-1-2016

Local Field Enhancement On Demand Based On Hybrid Plasmonic Dielectric Directional Coupler

Kholod Adhem Adhem
Wayne State University,

Follow this and additional works at: https://digitalcommons.wayne.edu/oa_dissertations

 Part of the [Electrical and Computer Engineering Commons](#)

Recommended Citation

Adhem, Kholod Adhem, "Local Field Enhancement On Demand Based On Hybrid Plasmonic Dielectric Directional Coupler" (2016). *Wayne State University Dissertations*. 1615.
https://digitalcommons.wayne.edu/oa_dissertations/1615

This Open Access Dissertation is brought to you for free and open access by DigitalCommons@WayneState. It has been accepted for inclusion in Wayne State University Dissertations by an authorized administrator of DigitalCommons@WayneState.

**LOCAL FIELD ENHANCEMENT ON DEMAND BASED ON
HYBRID PLASMONIC-DIELECTRIC DIRECTIONAL
COUPLER**

by

KHOLOD ADHEM

DISSERTATION

Submitted to the Graduate School

of Wayne State University,

Detroit, Michigan

in partial fulfillment of the

requirements for the degree of

DOCTOR OF PHILOSOPHY

2016

MAJOR: ELECTRICAL ENGINEERING

Approved By:

Advisor

Date

© COPYRIGHT BY

KHOLOD ADHEM

2016

All Rights Reserved

DEDICATION

Dedicated to

To my husband, Rami Allababneh, and daughter, Natali Allababneh,
who I love endlessly.

&

To my mother, Ahlam Laradi and my father, Zuhir Adhem, my inspiration
for strength, kindness and love.

ACKNOWLEDGEMENTS

I would thank Allah, for having made everything possible, by giving me the strength, patience and courage to complete this work.

I also would like to express my sincere thanks and appreciation to Professor Ivan Avrutsky for his continuous support, advice and guidance which contributed tremendous time to correct my research path. Appreciation is also due to Dr. Syed Mahmud, Dr. Mumtaz Usmen for their constructive comments and guide. Special thanks are due to Dr. Mark Cheng for supporting the research with an updated version of Comsol Multiphysics that had a great positive impact on the research progress.

Also, I would like to thank fellow graduate students in the Integrated Optics and Nanophotonic Lab, Sabarish Chandramohan, Mohammad Hossain, Eray Hasan for their support and cooperation. I also thank all the PhD Office staff for their help. I extend my thanks to the ECE department secretary, Dories R. Ferrise who was always there for me.

My special thanks to my classmates and graduate students, Aby Konampurath george, Ishan Jindal, and Mosad Alkhathami for their ever good company, cheering and support during the final days.

I thank all my friends and family especially my Father (Zuhier Adhem), Brother (Abdussalam and Kosay), and Sisters (Nora and Zain) for the love, encouragement and good spirits.

PREFACE

In this dissertation, I present my work on local field enhancement on demand based on hybrid plasmonic-dielectric directional coupler. The first part of the dissertation provides a detailed background on basic systems. It discusses the structure, the dispersion equation and the existing modes in a dielectric medium, two-layer (conductor-dielectric) (CD) system, and three-layer (conductor-gap-dielectric) (CGD) system. In the second part of the dissertation, I presented the structure of the conductor-gap-dielectric-substrate (CGDS) waveguide system. In this part, the design parameters, the dispersion equation and the guided modes in the CGDS system are studied. This part presents the phenomena of the local field enhancement on demand using the CGDS system; where a metal-tip is placed at the desirable location using AFM-style nano-positioners. In the third part of the dissertation, I presented possible integrated systems utilizing the CGDS structure. In the final part of my dissertation, I have presented a comprehensive analysis and study of the dispersion equation in the CGDS system.

Chapter 1 begins with an introduction of the electromagnetic description of guided modes in basic systems. It describes in details the basic structures: dielectric medium, CD system, CGD system. This section provides details about the derivation of the dispersion equation, and the modes analysis in each system.

Chapter 2 introduces the CGDS system, the very subject of this dissertation. It provides details about electromagnetic waves description, dispersion relation and existing guided modes in the structure.

Chapter 3 describes the field exchange and performance analysis in the CGDS system. It introduces the concept of local field enhancement on demand in the hybrid plasmonic-dielectric (CGDS) system. Chapter 3 also provides details about the amount of losses existing in the system. The final part of chapter 2 concludes that the hybrid CGDS waveguide made provides strong local field enhancement along with relatively low losses due to the short plasmonic coupling length. This explains why the CGDS system is an interesting and promising in the field of Nanophotonics and Integrated Optics.

Chapter 4 describes possible Optical Integrated systems utilizing the CGDS structure. An example of an overall system is an on-chip optical spectrometer that would ultimately measure absorption/emission spectra of individual quantum objects. The CGDS system also opens doors to other applications. For instance, biomedical applications using the visible spectral range and other applications in the invisible spectral range like a communication wavelength at 1550nm.

Chapter 5 discusses all possible guided modes in the CGDS system. It explains why the CGDS is a comprehensive system. It also provides details about that electric and magnetic field profiles at any point on the dispersion curves.

Chapter 6 is a conclusion that summarizes the concept of strong Local field enhancement on demand based on the vertical directional coupling between plasmonic mode and dielectric mode in the CGDS system. It describes the novelty and importance of the dispersion equation in the hybrid CGDS system. Dispersion equation has been derived analytically and solved numerically. It discusses some of the possible

applications requiring light-matter enhanced interactions in the visible range of wavelength spectrum.

Sincerely

Kholod Adhem

TABLE OF CONTENTS

| | |
|--|-----|
| Dedication | ii |
| Acknowledgements | iii |
| Preface | iv |
| Table of Contents | vii |
| List of Figures | x |
| Chapter 1. Introduction to Electromagnetic Description of Guided Modes | 1 |
| 1.1. Electromagnetic Waves in the Dielectric Medium | 3 |
| 1.2. Dispersion Equation in the Dielectric Medium | 5 |
| 1.3. Electromagnetic Waves in the Conductor-Dielectric (CD) System | 5 |
| 1.4. Dispersion Equation in the Conductor-Dielectric (CD) System | 8 |
| 1.5. Modes in the Conductor-Dielectric (CD) System | 9 |
| 1.6. Electromagnetic Waves in the Conductor-Gap-Dielectric (CGD) System | 11 |
| 1.7. Dispersion Equation in the Conductor-Gap-Dielectric (CGD) System | 13 |
| 1.8. Modes in the Conductor-Gap-Dielectric (CGD) System | 14 |
| 1.9. Conclusion | 15 |
| Chapter 2. Analytical Study of the Conductor-Gap-Dielectric-Substrate (CGDS) System | 16 |
| 2.1. Literature Review | 16 |
| 2.2. Electromagnetic Waves in the CGDS System | 18 |
| 2.3. Dispersion Equation of the CGDS System | 21 |
| 2.4. Mode Analysis in the CGDS System | 22 |

| | |
|--|----|
| 2.5. Conclusion | 26 |
| Chapter 3 Simulation and Results..... | 27 |
| 3.1. Simulation of Modes in the CGDS System | 27 |
| 3.2. Field Exchange in the CGDS System..... | 28 |
| 3.3. 3-D Version of the CGDS System..... | 29 |
| 3.4. Comparison Between Before and After Adding Conductor Layer to the CGD System..... | 31 |
| 3.5. Local Field Enhancement in the CGDS Structure | 32 |
| 3.6. Multi-Field Enhancement in the CGDS Structure..... | 34 |
| 3.7. Conclusion | 36 |
| Chapter 4. Applications of the CGDS System..... | 37 |
| 4.1. General Applications | 37 |
| 4.2. Possible System | 37 |
| 4.3. Advantages of Field Enhancement of the CGDS System Over Other Techniques | 40 |
| 4.4. Conclusion | 40 |
| Chapter 5. Comprehensive Analysis of the Dispersion Equation in the CGDS System | 41 |
| 5.1. Guided Modes in the CGDS with Film thickness in the micro-meter range..... | 41 |
| 5.2. Comparison Between Dispersion Relation in the CGD and CGDS Systems..... | 43 |
| 5.3. Electromagnetic Field Analysis and Simulation in the CGDS System | 46 |
| 5.4. Conclusion | 50 |
| Chapter 6. Conclusion..... | 52 |

| | |
|--|----|
| 6.1. Conclusion | 52 |
| Appendix A Matlab Script to Plot the Dispersion Relation for the Metal-Cladding and Thin-Film Waveguides | 53 |
| Appendix B Matlab Script to Calculate and Plot the Electric and Magnetic Fields at Any Value of Modal Indices on the Dispersion Relation Curves..... | 55 |
| References..... | 58 |
| Abstract..... | 65 |
| Autobiographical Statement..... | 67 |

LIST OF FIGURES

| | |
|---|----|
| Figure 1.1: Planar waveguide structure and x is the direction of the propagating wave | 3 |
| Figure 1.2: Schematic diagram of the conductor-dielectric structure..... | 6 |
| Figure 1.3: Schematic diagram of the conductor-gap-dielectric structure depicting the electric field norm..... | 11 |
| Figure 1.4: Schematic view of the conductor-gap-dielectric (CGD) system. (a) Slab conductor, (b) Sphere conductor, (c) Wedge conductor and (d) Cylindrical conductor | 12 |
| Figure 2.1: (a) Schematic view of the conductor-gap-dielectric-substrate (CGDS) structure. (b) Structure with magnetic field profile along different layers. | 19 |
| Figure 2.2: Modal indices of the two eigenmodes versus gap thickness, materials from top to bottom are Ag, air, SiO ₂ -TiO ₂ , and SiO ₂ at $\lambda = 632.8$ nm respectively. Film thickness= 500nm..... | 23 |
| Figure 3.1: Electric field component of (a) the TM-quasi-even and (c) the TM-quasi-odd modes supported by the hybrid coupler. (b) and (d) are corresponding electric field at $y=0.25$ μm in the y - z plane | 27 |
| Figure 3.2: (a) Light intensity profile along x - z plane corresponds to $y = 0.25$ μm . (b) Periodic energy exchange along the propagation length x | 29 |
| Figure 3.3: Schematic diagram of the hybrid directional coupler. The green region denotes SiO ₂ , the red region denotes (SiO ₂ -TiO ₂), and the gray region denotes Ag. x is the light propagation direction..... | 30 |
| Figure 3.4: Electric field component E_z of (a) the silica-titania dielectric mode in the y - z plane. (b) The corresponding E_z profile at $y = 0.25$ μm along $x = 0$. (c) Electric field component E_z of the coupled mode at $t_g = 17$ nm and (d) The corresponding electric field E_z profile at $y = 0.25$ μm along $x = 0$ | 31 |
| Figure 3.5: (a) Relative intensity of light along $x - z$ plane corresponds to $y = 0.25$ μm . (b) Light intensity in the gap along the propagation length x . (c) | |

| | | |
|--------------|--|----|
| | Power flux for the dielectric film mode at the input port ($x = 0 \mu\text{m}$) and at the output port ($x = 34.2 \mu\text{m}$) | 33 |
| Figure 3.6: | (a) Relative intensity of light along $x - z$ plane corresponds to $y = 0.25 \mu\text{m}$. (b) Light intensity in the multiple gaps along the propagation length x . (c) Power flux for the dielectric film mode at $x = 9.3 \mu\text{m}$, $x = 19.3 \mu\text{m}$, and $x = 29.3 \mu\text{m}$ | 35 |
| Figure 4.1: | Concept of an integrated optical device for the spectroscopy of a single molecule using local field enhancement based on hybrid plasmonic-dielectric waveguide directional coupler..... | 38 |
| Figure 5.1: | Structure of the CGDS system composed of all basic structures | 41 |
| Figure 5.2: | (a) Dispersion relation surface plot for the Metal-Cladding waveguide. (b) Modes in the Metal-Cladding waveguide with dielectric layer thickness of $2\mu\text{m}$ | 44 |
| Figure 5.3: | (a) Dispersion relation surface plot for the Thin-Film waveguide. (b) Modes in the Thin-Film waveguide with dielectric layer thickness of $2\mu\text{m}$ | 44 |
| Figure. 5.4: | Modal indices of guided modes versus gap thickness, materials from top to bottom are Ag, air, $\text{SiO}_2\text{-TiO}_2$, and SiO_2 at $\lambda = 632.8 \text{ nm}$ respectively. Film thickness= $2\mu\text{m}$ | 45 |
| Figure 5.5: | Field Strength, a.u. for the fundamental mode ($m=0$). (a) and (b): $t_g = 10^{-4} \mu\text{m}$ for $n_1^* = 1.971$.(c) and (d): $t_g = 0.017 \mu\text{m}$ for $n_1^* = 1.764$ and (e) and (f): $t_g = 10 \mu\text{m}$ for $n_1^* = 1.764$ | 49 |
| Figure 5.6: | Field Strength, a.u. for the first order mode ($m=1$). (a) and (b): $t_g = 10^{-4} \mu\text{m}$ for $n_1^* = 1.763$.(c) and (d): $t_g = 0.017 \mu\text{m}$ for $n_1^* = 1.744$ and (e) and (f): $t_g = 10 \mu\text{m}$ for $n_1^* = 1.744$ | 50 |

CHAPTER 1 INTRODUCTION TO ELECTROMAGNETIC DESCRIPTION OF GUIDED MODES

The interaction between photons and atoms or molecules determine the performance of optical devices [1]. The delocalized nature of photons prevent a single photon-atom interaction and hence the efficiency of optical and optoelectronic devices have been limited [2]. Many technical solutions to enhance device performance have been proposed [3-7]. One key is to come up with a novel structure that exhibits a strong light-matter interaction. Controlling light-matter interaction on the nanoscale are achieved by many optical nanoantenna structures [8, 9]. For instance; nanoparticle optical antenna [10, 11], nanorod optical antenna [12] and nano-bowtie optical antenna [13]. Although these types of nanoantennas provide a solution to light-matter enhancement problem, the presence of the antenna metal arms affects the very nature of the nano-scale object itself.

Some other approaches use ring resonators in which a metal cavity is placed close to the surface of the waveguide [14]. Photons carried by the waveguide is then get recycled in the ring cavity for a relatively long time ($10^4 - 10^8$) round trips and meanwhile interact with quantum dots placed on the surface of the proposed cavity [15]. Although this approach is also solving the problem of light-matter enhancement interaction, it is more like a recycling process for the photons. The relatively long time the process takes prevents an instantaneous photon-matter interaction. Moreover, the dynamic interaction between photons and quantum dots is changing.

As of today, there is no technical solution for an instantaneous single photon-matter interaction without affecting the nature or shape of atoms or molecules. In this dissertation work, a nano-focusing technique is presented. The concept of local field enhancement on demand allows strong instantaneous photon-matter interaction. The novelty of the structure is that the nano-scale metallic tip is approaching the top surface of a waveguide only when needed to create a high intensity on-demand electric field. This method thus does not affect the shape or nature of atoms placed on the surface of a waveguide.

To study guided modes in optical waveguide structures, we first need to apply Maxwell's equations [16] to the interface of two-layer (conductor-dielectric) system.

$$\nabla \times E = -\frac{\partial B}{\partial t}, \quad (1.1)$$

$$\nabla \times H = J_e + \frac{\partial D}{\partial t}, \quad (1.2)$$

$$\nabla \cdot D = \rho_e, \quad (1.3)$$

$$\nabla \cdot B = 0, \quad (1.4)$$

Where E and H are the electric and magnetic fields due to the external charge and current densities ρ_e and J_e respectively. D is the electric flux density and B is the magnetic flux density. Using the equations above, one can find the electromagnetic wave propagating in a homogeneous, isotropic and non-magnetic medium. In the assumption of no external charge and current density, we find,

$$\nabla \times \nabla \times E = -\mu_0 \frac{\partial^2 D}{\partial t^2} \quad (1.5)$$

If we assume that the dielectric profile is invariant along the structure, then equation above can be written as:

$$\nabla^2 E - \frac{\varepsilon}{c^2} \frac{\partial^2 E}{\partial t^2} = 0, \quad (1.6)$$

Where c is the speed of light in vacuum. Assume time dependence for the electric field then we can write:

$$E(r, t) = E(r)e^{-i\omega t}, \quad (1.7)$$

where ω is the angular frequency. Therefore, the wave equation can be written as:

$$\nabla^2 E + k_o^2 \varepsilon E = 0 \quad (1.8)$$

The above equation is well known as Helmholtz equation, where k_o is the wave vector in free space.

1.1 Electromagnetic Waves in the Dielectric Medium

Figure (1.1) depicts a dielectric medium with positive real dielectric permittivity ε . Assume x is the wave propagation direction and no electric or magnetic field variation along the y -axis.

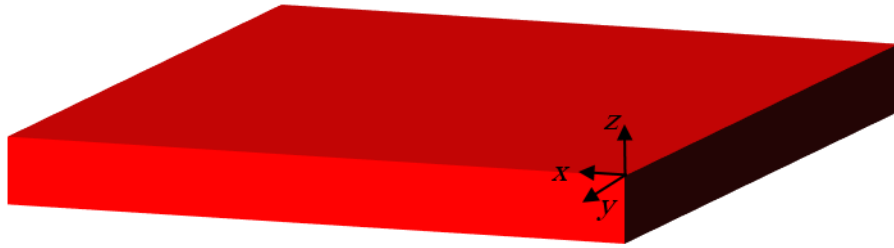


Figure 1.1: Planar waveguide structure and x is the direction of the propagating wave.

Consider $z = 0$ as the surface of the dielectric medium, the electromagnetic wave in the structure can be expressed as follows:

$$E(x, y, z) = E(z)e^{ik_x x}, \quad (1.9)$$

where k_x is the x -component of the wave vector. By plugging equation (1.9) into Helmholtz equation (1.8), one can find:

$$\frac{\partial^2 E}{\partial z^2} + (k_o^2 \varepsilon - k_x^2)E = 0. \quad (1.10)$$

Similarly, the equation for the magnetic field H can be obtained [17, 18]. For a TM mode, we only have three components for the electric and magnetic fields (H_y, E_x, E_z). As there is only one magnetic field component when considering TM mode, it is always easier to start with the magnetic field expression. The magnetic field equation can be written as:

$$\frac{\partial^2 H_y}{\partial z^2} + (k_o^2 \varepsilon - k_x^2)H_y = 0, \quad (1.11)$$

and electric field components can be expressed as:

$$E_x = -i \frac{1}{\omega \varepsilon_0 \varepsilon} \frac{\partial H_y}{\partial z} \quad (1.12)$$

$$E_z = -\frac{k_x}{\omega \varepsilon_0 \varepsilon} H_y \quad (1.13)$$

Similarly, for the TE mode we have only three components for the electric and magnetic fields (E_y, H_x, H_z). The equations for the electric and magnetic fields becomes:

$$\frac{\partial^2 E_y}{\partial z^2} + (k_o^2 \varepsilon - k_x^2) E_y = 0 \quad (1.14)$$

$$H_x = i \frac{1}{\omega \mu_0} \frac{\partial E_y}{\partial z} \quad (1.15)$$

$$H_z = \frac{k_x}{\omega \mu_0} E_y \quad (1.16)$$

1.2 Dispersion Equation in the Dielectric Medium

Dispersion equation is an important relation that contains a lot of information about the propagating wave [19]. It is defined as the relationship between the wave vector and the angular frequency. Its simplest form in free space is

$$k_o = \frac{\omega}{c}, \quad (1.17)$$

where c is the speed of light in free space. For a medium with permittivity ε_d , the wave vector becomes $k = k_o \sqrt{\varepsilon_d}$. Thus, the dispersion equation in a medium with permittivity ε_d can be written as:

$$k = \frac{\omega}{c} \sqrt{\varepsilon_d}, \quad (1.18)$$

1.3 Electromagnetic Waves in the Conductor-Dielectric System

Figure (1.2) shows a two-layer system consists of the upper conductor layer ($z > 0$) with a complex permittivity $\varepsilon_c(\omega)$ and a dielectric lower layer ($z < 0$) with a real positive permittivity ε_d . The existing mode at the interface is called the surface plasmon polariton (SPP). SPP mode is a TM-polarized mode in nature. To be specific, the

propagation direction is along the x -axis and the magnetic field is polarized in the y -direction.

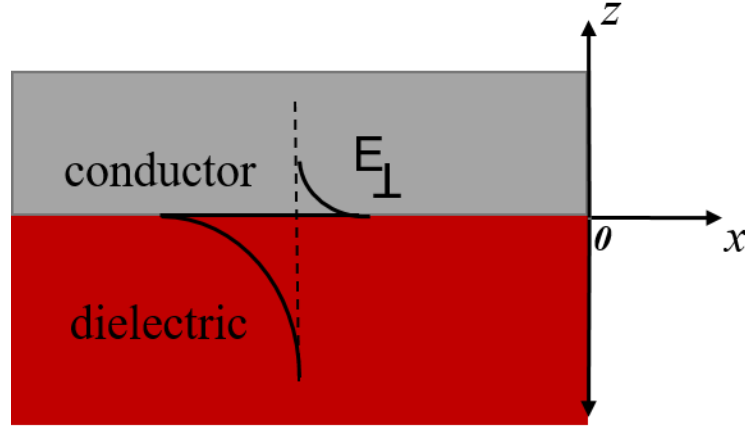


Figure 1.2: Schematic diagram of the conductor-dielectric structure.

Here, the structure is variant in the z -direction meaning that the magnetic field profile is changing along the z -axis. In this system, we only have one boundary at the interface between the conductor and the dielectric at $z = 0$. The wave vector k consists of its Cartesian components as:

$$k^2 = k_x^2 + k_y^2 + k_z^2 = \epsilon k_o^2, \quad (1.19)$$

where $k_o = \frac{2\pi}{\lambda}$ is the wave vector in free space. The magnetic field is not changing along the y -axis, we can set $k_y = 0$. The z -component of the wave vector thus can be expressed as:

$$k_z = \pm \sqrt{\epsilon k_o^2 - k_x^2}, \quad (1.20)$$

where $k_x^2 = \epsilon^* k_o^2 = n^* k_o^2$ in which ϵ^* and n^* are the effective permittivity and effective modal index respectively. Therefore, k_z can be rewritten as:

$$k_z = \pm k_o \sqrt{\epsilon - n^{*2}} \quad (1.21)$$

For the upper conductor layer, ($z > 0$), the z -component of the wave vector becomes:

$$k_z = \pm k_o \sqrt{n_c^2 - n^{*2}} \quad (1.22)$$

Since $n_c < n^*$, the quantity under the square root is negative and the k_z returns an imaginary quantity. One can define r as the quantity related to the z -component of the wave vector as follows:

$$r = k_o \sqrt{n^{*2} - n_c^2} \quad (1.23)$$

Finally k_z can be written as $k_z = \pm ir$. The normal component of the electric field profile in the conductor-dielectric system is also shown in figure (1.2).

Similarly, $n_d < n^*$, and from equation (1.21) we can define the quantity p as a quantity related to the z -component of the wave vector as follows:

$$p = k_o \sqrt{n^{*2} - n_d^2} \quad (1.24)$$

Since the magnetic field will be decaying into the conductor layer as well as into the dielectric layer, one can write the magnetic field equations as follows:

$$H_y(x, z) = Ae^{-rz} \cdot e^{ik_x \cdot x} \quad \text{for } z > 0 \quad (1.25)$$

$$H_y(x, z) = Be^{-pz} \cdot e^{ik_x \cdot x} \quad \text{for } z < 0 \quad (1.26)$$

Similar equations can be obtained for the x -component of the electric field using

$$E_x \sim \frac{1}{\epsilon} \frac{\partial H_y}{\partial z} \text{ as follows:}$$

$$\frac{-r}{\epsilon_c} A e^{-rz} \cdot e^{ik_x x} \quad \text{for } z > 0 \quad (1.27)$$

$$\frac{-p}{\epsilon_d} B e^{-pz} \cdot e^{ik_x x} \quad \text{for } z < 0 \quad (1.28)$$

1.4 Dispersion Equation in the Conductor-Dielectric System

Solving the equations in the previous section, one can obtain the dispersion equation in the two-layer (conductor-dielectric) system. Boundary conditions state that tangent components of electric and magnetic fields must be continuous at the interface.

This means that E_t and H_t are continuous. Since $H_{t_1} = H_{t_2}$ at $z = 0$ then,

$$A e^{-rz} = B e^{-pz}, \quad (1.29)$$

And $E_{t_1} = E_{t_2}$ at $z = 0$ then,

$$\frac{-r}{\epsilon_c} A e^{-rz} = \frac{-p}{\epsilon_d} B e^{-pz}. \quad (1.30)$$

Divide equation (1.29) by equation (1.30)

$$\frac{r}{\epsilon_c} = \frac{p}{\epsilon_d} \quad (1.31)$$

We get,

$$\frac{\epsilon_c}{k_o \sqrt{n^{*2} - \epsilon_c}} = \frac{\epsilon_d}{k_o \sqrt{n^{*2} - \epsilon_d}} \quad (1.32)$$

Thus, the dispersion equation for the two-layer system can be written as [20, 21]:

$$k_x = k_o \sqrt{\frac{\epsilon_d \epsilon_c}{\epsilon_d + \epsilon_c}} \quad (1.33)$$

1.5 Modes in the Conductor-Dielectric System

The conductor-dielectric structure supports only plasmonic mode (so-called surface plasmon polariton). The plasmonic mode is a TM-polarized mode perpendicular to the interface between the conductor and the dielectric layers. The modal index of each layer is defined as the square root of the layer permittivity. The modal index is n_d and n_c for the dielectric and the conductor layers respectively. The effective modal index of such a structure can be expressed as:

$$n_{spp} = \sqrt{\frac{\varepsilon_d \times \varepsilon_c}{\varepsilon_d + \varepsilon_c}}, \quad (1.34)$$

Where ε_d and ε_c are the permittivities of the dielectric and conductor layers respectively. It is important to mention that the real part of the effective modal index of this structure ($\text{Re } n_{spp}$) is always greater than the dielectric modal index (n_d). For instance, if $\lambda=0.6328 \mu\text{m}$, the permittivity of gold at this particular wavelength is $\varepsilon_c = -15.822 + 1.075i$ [22]. Assume an air dielectric medium with a modal index equals to $n_d = 1.0$. The real part of the effective modal index ($\text{Re } n_{spp}$) using equation (1.34) is equal to 1.03301. Thus, it is slightly larger than $n_d = 1.0$.

The propagation length is defined as the length the SPP travels before its intensity is attenuated to 1/e of its initial value. The propagation length for the dielectric-conductor structure is given by [23]:

$$L_p = \frac{\lambda}{4\pi \text{Im}(n_{spp})}, \quad (1.35)$$

Using the numerical values above, the SPP propagation length was found to be equal to 21.4 μm . The corresponding propagation loss of SPP is given by:

$$\alpha_p = \frac{4\pi \text{Im}(n_{spp})}{\lambda}, \quad (1.36)$$

Similarly, using the same numerical values used above, the propagation loss in the conductor-dielectric system is found to be equal to 0.0468 $1/\mu\text{m}$.

The field penetration depth in the dielectric layer is approximated as [23]:

$$L_d = \left(\frac{\lambda}{2\pi}\right) \frac{1}{\text{Re}(\sqrt{n_{spp}^2 - n_d^2})}, \quad (1.37)$$

Substituting the above numerical values, the field penetration depth in the dielectric layer is found to be equals to 0.388 μm . Hence; the penetration depth is inversely proportional to the index of the dielectric layer $\sim (1/n_d^2)$. Thus; for higher-index materials, the penetration depth is very small. Therefore, the plasmon field will be tightly confined to the interface and this is a very desirable case. In a similar manner, the field penetration depth in the conductor layer is approximated as [24]:

$$L_c = \left(\frac{\lambda}{2\pi}\right) \frac{1}{\text{Re}(\sqrt{n_{spp}^2 - n_c^2})}, \quad (1.38)$$

Substituting the same above numerical values one can find the penetration depth in the conductor layer to be equal to 0.0244 μm . It concludes that for the conductor layer, the confined mode is tighter and the field dies much quicker than in the dielectric layer. The bottom line is that SPP mode existing at the interface between a conductor and a dielectric layers will have high losses due to the imaginary part of the conductor

modal index (n_c). SPP mode will also have strong field confinement when using high-index materials.

1.6 Electromagnetic Waves in the Conductor-Gap-Dielectric system

Figure (1.3) depicts a three-layer (conductor-gap-dielectric) system. The top layer is a conductor. The lower layer is a high index dielectric, and the sandwiched layer is a low index dielectric layer we call it the gap. Figure (1.3) also depicts the normal component of the electric field in the structure.

Assume the wave propagates in the x -direction. The magnetic field is polarized in the y -direction. The structure is variant in the z -direction, meaning that the magnetic field profile is changing along the vertical z -axis.

In this system, we have two boundaries. One between the conductor and the gap at $z = t_g$. The other boundary is located between the gap and the high-index dielectric layer at $z = 0$.

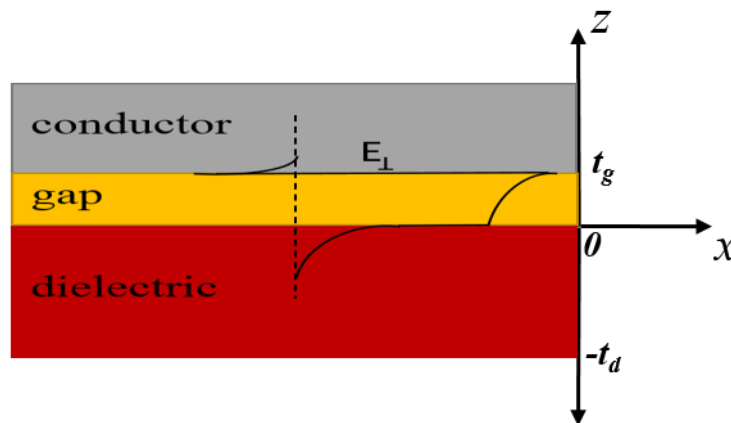


Figure 1.3: Schematic diagram of the conductor-gap-dielectric structure depicting the electric field norm.

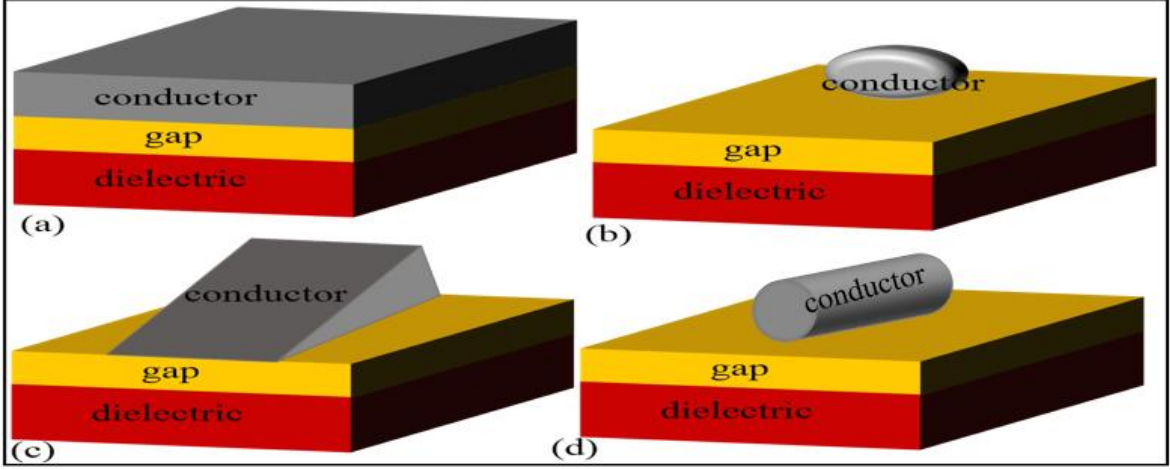


Figure 1.4: Schematic view of the conductor-gap-dielectric (CGD) system. (a) Slab conductor, (b) Sphere conductor, (c) Wedge conductor and (d) Cylindrical conductor.

Figure (1.4) shows different schematic views for the three-layer system; where the conductor layer can be of different shapes: slab, sphere, and wedge or cylindrical. These arrangements can tightly confine and guide light in a nanoscale gap far beyond the diffraction limit of light.

The magnetic field equation for the conductor-gap-dielectric system from top to bottom can be written as follows:

$$H_y(x, z) = Ae^{-r(z-t_g)} e^{ik_x \cdot x} \quad \text{for } z > t_g \quad (1.39)$$

$$H_y(x, z) = [Be^{+q(z-t_g)} + Ce^{-qz}] e^{ik_x \cdot x} \quad \text{for } 0 < z < t_g \quad (1.40)$$

$$H_y(x, z) = De^{+pz} e^{ik_x \cdot x} \quad \text{for } z < 0 \quad (1.41)$$

Where r , q , and p are quantities related to the z -component of the wave vector, and are defined as follows:

$$r = k_o \sqrt{n^{*2} - n_c^2}, \quad q = k_o \sqrt{n^{*2} - n_g^2}, \quad p = k_o \sqrt{n^{*2} - n_d^2} \quad (1.42)$$

Similar equations can be obtained for the x -component of the electric field using

$E_x \sim \frac{1}{\varepsilon} \frac{\partial H_y}{\partial z}$ as follows:

$$\frac{-r}{\varepsilon_c} A e^{-r(z-t_g)} \quad \text{for } z > t_g \quad (1.43)$$

$$\frac{q}{\varepsilon_g} [B e^{+q(z-t_g)} - C e^{-qz}] \quad \text{for } 0 < z < t_g \quad (1.44)$$

$$\frac{p}{\varepsilon_d} D e^{pz} \quad \text{for } z < 0 \quad (1.45)$$

1.7 Dispersion Equation in the Conductor-Gap-Dielectric System

To obtain the dispersion relation for the three-layer system, match boundary conditions (H_y is continuous, and derivative of H_y divided by ε is continuous):

$$H_y(z > t_g) = H_y(0 < z < t_g) \quad (1.46)$$

$$H_y(0 < z < t_g) = H_y(z < 0) \quad (1.47)$$

$$\frac{1}{\varepsilon} \frac{\partial H_y}{\partial z}(z > t_g) = \frac{1}{\varepsilon} \frac{\partial H_y}{\partial z}(0 < z < t_g) \quad (1.48)$$

$$\frac{1}{\varepsilon} \frac{\partial H_y}{\partial z}(0 < z < t_g) = \frac{1}{\varepsilon} \frac{\partial H_y}{\partial z}(z < 0) \quad (1.49)$$

Substituting equations (1.46) through (1.49) into equations (1.39) through (1.45), we get:

$$A = B + C e^{-qt_g} \quad (1.50)$$

$$B e^{-qt_g} + C = D \quad (1.51)$$

$$\frac{-r}{\varepsilon_c} A = \frac{q}{\varepsilon_g} [B - C e^{-qt_g}] \quad (1.52)$$

$$\frac{q}{\varepsilon_g} [B e^{-qt_g} - C] = \frac{p}{\varepsilon_d} D \quad (1.53)$$

Solving the four equations (1.50) through (1.53), one can find out the dispersion equation for the CGD system as follows:

$$e^{-qt_g} \left(\frac{q}{\varepsilon_g} - \frac{r}{\varepsilon_c} \right) \cdot \left(\frac{q}{\varepsilon_g} - \frac{p}{\varepsilon_d} \right) - \left(\frac{q}{\varepsilon_g} + \frac{r}{\varepsilon_c} \right) \left(\frac{q}{\varepsilon_g} + \frac{p}{\varepsilon_d} \right) = 0 \quad (1.54)$$

1.8 Modes in the Conductor-Gap-Dielectric (CGD) System

As mentioned earlier, CGD system structure is composed of a low-index dielectric gap with a permittivity ε_g and a thickness t_g . On the top of the gap there is a semi-infinite conductor layer with a complex permittivity $\varepsilon_c = \varepsilon' + i\varepsilon''$. Below the gap there is a semi-infinite high index dielectric layer with a permittivity of ε_d . The effective modal index becomes n_{CGD} [25] and it is now a function of the gap thickness. The n_{CGD} is related to n_{SPP} as follows:

$$n_{CGD} \Big|_{t_g=0} = n_{SPP} = \sqrt{\frac{\varepsilon_d \times \varepsilon_c}{\varepsilon_d + \varepsilon_c}} \quad (1.55)$$

The modal index n_{CGD} can be obtained by solving the dispersion equation of the CGD system found from the previous section. Obviously, we cannot provide an accurate and explicit expression for the effective modal index in the three-layer system because the effective modal index term is embedded into the dispersion equation. One can set a specific gap layer thickness t_g and use the 'root' function `fzero` from Matlab to find the exact solutions of the dispersion equation (effective modal indices for the structure).

Changing the gap layer thickness will lead to a different solution each time. Therefore, one can sweep the gap thickness along a desired range and calculate the n_{CGD} for the whole gap range.

1.9 Conclusion

The electromagnetic wave equations, the dispersion relation and the guided modes in the two-layer (conductor-dielectric) and three-layer (conductor-gap-dielectric) systems are presented in details to provide a basic background to introduce the structure of the four-layer (conductor-gap-dielectric-substrate) (CGDS) system, the very subject of this dissertation. Examples of some numerical calculations for the CD and CGD systems are provided to understand some about the theoretical analysis of these basic block systems.

CHAPTER 2 INTRODUCTION TO THE CONDUCTOR-GAP-DIELECTRIC-SUBSTRATE SYSTEM

Massive size mismatch between dimensions of integrated photonic components and integrated electronics has been one of the greatest challenges in integrated optics for years [26]. Plasmonics provides a solution to this problem. Plasmonic waveguides could be used to guide signals that propagate at optical frequencies. Unlike the dielectric waveguides, plasmonic waveguides can confine light far beyond the diffraction limit of light [27]. However, plasmonic waveguides suffer from high losses due to absorption in metal. In contrast, conventional dielectric waveguides, at least in principle, are low-loss waveguides. Modern technology requires a structure that offers both high confinement and low loss. Thus, the integration of plasmonic-dielectric waveguide directional couplers has been a subject of attention to many researchers [28, 29].

The concept of local field enhancement using conductor-gap-dielectric-substrate (CGDS) waveguide structure is proposed in this work. The mechanism of the CGDS works as follows: Light waves are guided by conventional nearly lossless dielectric waveguides and, upon demand, they are transformed into highly confined plasmonic modes with strong local field enhancement, and get transformed back into low-loss dielectric modes. The concept is illustrated by numerical simulations using a commercial finite-element package from COMSOL Multiphysics.

2.1 Literature Review

Signal routing between plasmonic modes and dielectric modes in plasmonic integrated circuits (PIC) has been reported in [30–34]. Currently, strongly confined

modes are achieved by many plasmonic waveguide structures such as the slot waveguide [35], the dielectric-loaded waveguide [36], the groove waveguide [37] and the hybrid waveguide [38]. Many technical solutions have been proposed to develop hybrid dielectric-plasmonic structures that would provide high confinement and moderate optical losses. As an example, a horizontal directional coupler between a plasmonic waveguide and a silicon dielectric waveguide has been reported in [39]. The study was to couple light from the dielectric mode of size 297 nm×340 nm to a plasmonic mode of a size 200 nm×40 nm. The propagation loss is found to be 0.052 dB/μm and the associated propagation length is 83 μm at a communication wavelength of $\lambda=1550$ nm. Vertical directional coupling has also been reported, in which signal routing between metal-insulator-metal (MIM) plasmonic waveguide and silicon dielectric waveguide was analyzed [40]. It was found that the hybrid coupler was able to couple light from the silicon dielectric waveguide with a dimension of 220 nm×260 nm to the upper arm MIM plasmonic waveguide with dimensions of 200 nm×150 nm. The propagation loss was found to be 0.36 dB/μm and the corresponding propagation length was 12 μm at 1550 nm wavelength. Overall, these studies indicate that the tradeoff between the degree of confinement and optical losses can be shifted in one or the other direction depending on what is more important for a particular application. Some applications, for instance, require that optical signals propagate for relatively large distances, on the order of few millimeters on a chip, while critical optical interactions are only feasible when the mode size is squeezed far beyond the diffraction limit. An example is an on-chip optical spectrometer that would ultimately measure

absorption/emission spectra of individual quantum objects, such as large molecules or quantum dots. As of now, there is no technical solution for an optical waveguide that would meet such demanding requirements. We propose here a concept of local optical confinement on demand. In this concept, light mostly is guided by nearly lossless dielectric waveguides, but once needed, the optical power of dielectric waveguide is transferred, almost completely, to a highly confined plasmonic mode, and then back to the dielectric mode. The concept is illustrated by numerical simulations using a commercial finite-element package from COMSOL Multiphysics.

The idea of the vertical directional coupler presented in this dissertation is inspired by the integrated optical polarizer device [41]. The functionality of the polarizer is to enable one polarization state (transverse magnetic (TM) or transverse electric (TE)) to propagate while the other polarization state is eliminated due to high propagation loss. Numerous types of waveguide polarizers have been realized over many years [42], including, for example, metal-clad waveguides [43]. We only deal with TM mode in our analysis throughout this work. In contrast to polarizers, the directional coupler used here is designed in such a way that losses are relatively low due to short interaction length.

2.2 Electromagnetic Waves in the Conductor-Gap-Dielectric-Substrate (CGDS) System

Figure (2.1) shows a four-layer system. The structure consists of following layers: conductor (metal) cover at the top, followed by a low-index dielectric gap, high-index dielectric film, and a dielectric substrate. The thickness of the gap layer is t_g , and

thickness of the dielectric film is t_d . The permittivities of the conductor, gap, dielectric film and substrate are ϵ_c , ϵ_g , ϵ_d , and ϵ_s . Cover and substrate are semi-infinite layers. The structure is only variant in the z -direction. The layers can be for instance: silver (Ag), a gap filled with air, silica-titania ($\text{SiO}_2\text{-TiO}_2$) film, and fused quartz SiO_2 substrate.

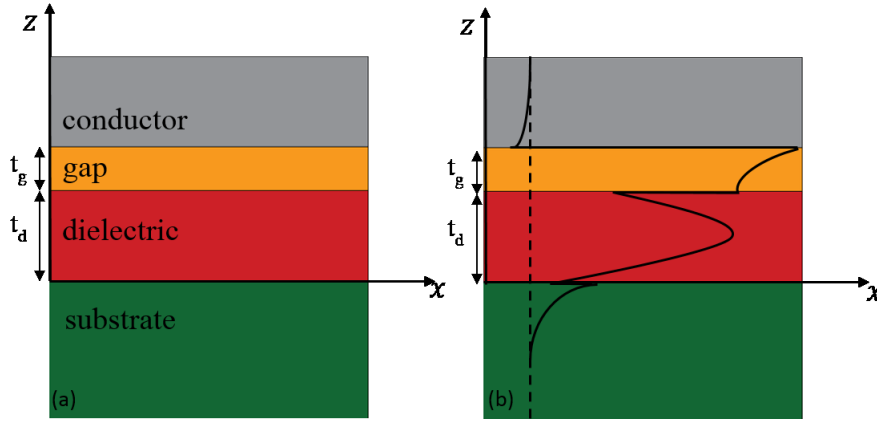


Figure 2.1: (a) Schematic view of the conductor-gap-dielectric-substrate (CGDS) structure. (b) Structure with magnetic field profile along different layers.

The structure is a hybrid waveguide that can be thought of as a combination of two waveguides. The first waveguide is a plasmonic waveguide formed by a conductor and gap layers, while the second waveguide is a high index contrast dielectric waveguide formed by the film sandwiched between the gap and the substrate. For a small gap thickness, the coupling between these two waveguides is strong. The plasmonic mode considered in this system is a TM mode in nature. In a structure with flat interfaces made of isotropic materials, it can only couple to TM modes of the dielectric film. Theoretical analysis of hybrid plasmonic waveguides has been extensively studied in [44].

Modes supported by the structure can be obtained by extending an earlier theoretical work on conductor-gap-dielectric waveguide [45, 46] by adding one more layer serving as a substrate for the film. The structure thus becomes conductor-gap-dielectric-substrate system (CGDS). Assuming propagation in the x -direction, the expressions for the magnetic H_y field component in all layers from top to bottom can be written as follows:

$$H_y(x, z) = Ae^{-r(z-t_g-t_d)} e^{ik_x \cdot x}, \quad \text{if } z \geq t_g + t_d \quad (2.1)$$

$$H_y(x, z) = [Be^{q(z-t_d)} + Ce^{-q(z-t_d)}] e^{ik_x \cdot x}, \quad \text{if } t_d \leq z \leq t_g + t_d \quad (2.2)$$

$$H_y(x, z) = [De^{(pz)} + Ee^{-(pz)}] e^{ik_x \cdot x}, \quad \text{if } 0 \leq z < t_d \quad (2.3)$$

$$H_y(x, z) = Fe^{sz} e^{ik_x \cdot x}, \quad \text{if } z < 0 \quad (2.4)$$

In the above equations r , q , p and s are related to the z -components of the wave-vector, and are given by:

$$r = k_o \sqrt{n^{*2} - \epsilon_c}, \quad q = k_o \sqrt{n^{*2} - \epsilon_g}, \quad p = k_o \sqrt{n^{*2} - \epsilon_d}, \quad s = k_o \sqrt{n^{*2} - \epsilon_s}, \quad (2.5)$$

where n^* is the modal index, and $k_o = \frac{2\pi}{\lambda}$ is the wave-vector in free space. In a case of

$n^* < \epsilon_d$, the p variable in equation (2.5) is pure imaginary quantity and equation (2.3)

turns in a combination of *sin* and *cos* functions. Similar equations can be obtained for

the x -component of the electric field using $E_x \sim \frac{1}{\epsilon_z} \frac{\partial H_y(z)}{\partial z}$

$$\frac{-r}{\epsilon_c} A e^{-r(z-t_g-t_d)} \quad (2.6)$$

$$\frac{q}{\epsilon_g} [B e^{+q(z-t_g)} - C e^{-q(z-t_g)}] \quad (2.7)$$

$$\frac{p}{\epsilon_d} [D e^{pz} - E e^{-pz}] \quad (2.8)$$

$$\frac{s}{\epsilon_s} F e^{sz} \quad (2.9)$$

2.3 Dispersion Equation of the Conductor-Gap-Dielectric-Substrate (CGDS) System

By applying appropriate boundary conditions (continuity of $H_y(z)$ and

$E_x \sim \frac{1}{\epsilon_z} \frac{\partial H_y(z)}{\partial z}$ across the interfaces at $z = t_d$ and $z = t_g + t_d$). The dispersion equation

for the modes in the CGDS system is found as:

$$\tanh(qt_g)(C_1 + C_2) - (A_1 + A_2) = 0, \quad (2.10)$$

where

$$A_1 = \left(\frac{r}{\epsilon_c} + \frac{p}{\epsilon_d}\right) \cdot \left(\frac{p}{\epsilon_d} + \frac{s}{\epsilon_s}\right) \quad (2.11)$$

$$A_2 = \left(\frac{r}{\epsilon_c} - \frac{p}{\epsilon_d}\right) \cdot \left(\frac{p}{\epsilon_d} - \frac{s}{\epsilon_s}\right) \cdot \exp(-2p.t_d) \quad (2.12)$$

$$C_1 = -\left(\frac{q}{\epsilon_g} + \frac{pr\epsilon_g}{\epsilon_d\epsilon_c q}\right) \cdot \left(\frac{p}{\epsilon_d} + \frac{s}{\epsilon_s}\right) \quad (2.13)$$

$$C_2 = -\left(\frac{q}{\epsilon_g} - \frac{pr\epsilon_g}{\epsilon_d\epsilon_c q}\right) \cdot \left(\frac{p}{\epsilon_d} - \frac{s}{\epsilon_s}\right) \cdot \exp(-2p.t_d) \quad (2.14)$$

2.4 Mode analysis in the Conductor-Gap-Dielectric-Substrate (CGDS) System

We numerically solve equation (2.10) with definitions in equations (2.5), (2.11) and (2.14) to find the exact solution for the modal indices n^* of the guided modes for various gap thicknesses at 632.8 nm wavelength. Various programming languages can be used for this purpose; we used the 'root' function of Mathcad as our choice. We compare the values obtained from the analytical method as described above to those obtained by the finite-element code, Comsol Multiphysics.

In Comsol, the following values are entered for the permittivities $\varepsilon_c = -15.822 + 1.075i$ [22], $\varepsilon_d = 3.13$, $\varepsilon_s = 2.1$ and $\varepsilon_g = 1.0$ for Ag, SiO₂-TiO₂, SiO₂ and air at $\lambda = 632.8$ nm respectively. The structural parameters selected in the simulation: $w_d = 500$ nm, $t_d = 500$ nm, $t_s = 760$ nm, $w_c = 500$ nm, $t_c = 304$ nm and $t_g = 17$ nm. Perfect Electric Conductor boundary conditions (PEC) are applied to all boundaries, and an extremely fine free triangular meshing is applied to the whole structure.

The effective indices predicted by the two methods matched well. Figure (2.2) provides the values of effective mode indices for the guided modes as a function of gap layer thickness t_g . The solid lines are obtained by the analytical method [solving equation (2.10) using Mathcad], and the points indicate the results from Comsol Multiphysics. Although the agreement between the analytical method and Comsol Multiphysics is also good in the whole range of gap layer thickness, we only show the range from [1 nm-100 nm] from Comsol.

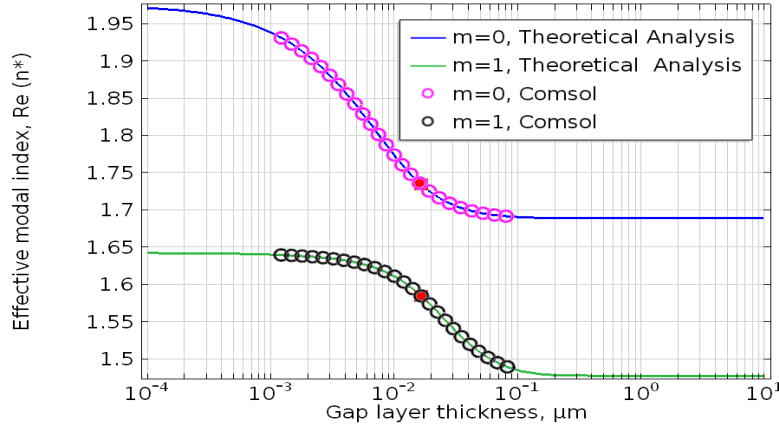


Figure 2.2: Modal indices of the two eigenmodes versus gap thickness, materials from top to bottom are Ag, air, SiO₂-TiO₂, and SiO₂ at $\lambda = 632.8$ nm respectively. Film thickness= 500nm.

The dispersion curves in figure (2.2) show the anti-crossing behavior typical for coupled modes. The plasmonic mode as such has a dispersion curve with a large negative slope. The anticrossing at $t_g = 17$ nm, where the difference between the indices takes on minimal value, indicates a strong interaction between the mode of the film and the plasmonic mode. The minimum modal index difference is depicted in figure (2.2) with red dots for each mode. Therefore, $t_g = 17$ nm is the gap size to be used in the rest of our analysis.

The CGDS structure with film thickness $t_d = 500$ nm supports two guided modes, the fundamental ($m = 0$), and the first order ($m = 1$) mode. At large values of t_g (greater than $1 \mu\text{m}$), the guided mode in the CGDS structure becomes the mode of the thin film waveguide with gap/substrate claddings. Thus, the modal indices for ($m = 0$), and ($m = 1$) equal to 1.688 and 1.477 respectively satisfy the dispersion equation of the thin film waveguide. Using the same notations in equation (2.5), the dispersion equation for the TM mode in a thin film waveguide [47] can be rewritten as:

$$p_d \cdot t_d - \tan^{-1}\left(\frac{\varepsilon_d Q}{\varepsilon_g p_d}\right) - \tan^{-1}\left(\frac{\varepsilon_d S}{\varepsilon_s p_d}\right) - m\pi = 0, \quad (2.15)$$

where $p_d = k_o \sqrt{\varepsilon_d - n^{*2}}$ is a pure real quantity, and can be written using notation in equation (2.5) as $p_d = -ip$.

At small values of t_g (less than 1 nm), the guided mode in the CGDS structure becomes the plasmonic mode of the metal-cladding waveguide with conductor/substrate claddings. The modal index of the fundamental ($m = 0$) mode becomes the modal index of the surface plasmon polariton (SPP) mode at the conductor/dielectric interface and can be obtained using [48]

$$\text{Re } n^* = \left(\frac{\varepsilon_c \cdot \varepsilon_d}{\varepsilon_c + \varepsilon_d}\right)^{1/2}, \quad (2.16)$$

Using $\varepsilon_c = -15.822 + 1.075i$ [22], and $\varepsilon_d = 3.13$, the real part of the effective modal index for ($m = 0$) is found to be equal to 1.974.

The first order ($m = 1$) mode is the mode of the dielectric film with conductor/substrate claddings. Its modal index equals to 1.642 satisfies the dispersion equation of the metal-cladding waveguide. Following the same notations in equation (2.5), the dispersion equation for the TM mode for the metal-cladding waveguide [47] can be rewritten as [49]:

$$p_d \cdot t_d - \tan^{-1}\left(\frac{\varepsilon_d R}{\varepsilon_c p_d}\right) - \tan^{-1}\left(\frac{\varepsilon_d S}{\varepsilon_s p_d}\right) - m\pi = 0, \quad (2.17)$$

Note that modal indices found from equations (2.15) and (2.17) match very well the limits at $t_g \rightarrow \infty$ and $t_g \rightarrow 0$ found from solving equation (2.10).

The plasmonic mode is a combination of the ($m = 0$) and ($m = 1$) supermodes. The optimal gap size is calculated such that the minimal modal indices difference between $m = 0$ and $m = 1$ occurs. Assume the materials from top to bottom are Ag, air, SiO₂-TiO₂, and SiO₂ at $\lambda = 632.8$ nm respectively. Film thickness = 500 nm. The propagation length of the plasmonic mode at the optimal gap size can be estimated according to [50]:

$$L_o = \frac{\lambda}{4\pi \operatorname{Im}\left(\frac{n_o^* + n_1^*}{2}\right)}, \quad (2.18)$$

where n_o^* and n_1^* the complex modal indices for ($m = 0$) and ($m = 1$) modes respectively. At gap thickness t_g equal to 17 nm, n_o^* is equal to $1.7338 + 0.0022i$ and n_1^* equals to $1.5843 + 0.0029i$. These values are denoted as red dots in the dispersion relation graph in figure (2.2). The propagation length L_o is found from equation (2.18) to be equal to 19.92 μm .

Propagation of coupled guided modes is often considered in terms of supermodes which are eigenmodes of the entire multilayer structure. Coupling between the film mode and the plasmonic mode forms two types of supermodes which later will be referred to as TM-quasi-even and TM-quasi-odd modes. They propagate along the CGDS structure with different propagation constants. The interference between the supermodes results in the electromagnetic field confined mainly to the film or to the gap depending on the relative phase of the supermodes. At a distance equal to the coupling length L_c , almost all energy of the dielectric film is getting transferred to the

gap mode. The coupling length is a measure of the beating length of the two eigenmodes, and it can be related to propagation constants by [51]:

$$L_c = \frac{\pi}{\beta_e - \beta_o}, \quad (2.19)$$

where β_e and β_o are the propagation constants for the TM-quasi-even and odd eigenmodes respectively.

The propagation constant is related to the modal index as $\beta = n^* k_o$. Hence at the optimal gap size 17nm, the L_c is equal to 2.1 μm . It concludes that the energy exchange between the two waveguides takes place every 2.1 μm , and that the one period is twice the coupling length and equals to 4.2 μm .

2.5 Conclusion

The electromagnetic wave equations, the dispersion relation, and the guided modes in the CGDS system are well presented. Examples of some numerical calculations in the structure are provided to add more details to the theoretical analysis of the guided modes. This analysis is necessary to introduce the concept of local field enhancement on demand using CGDS system in the next chapter.

CHAPTER 3 CONDUCTOR-GAP-DIELECTRIC-SUBSTRATE (CGDS) SYSTEM SIMULATION AND RESULTS

3.1 Simulation of Modes in the CGDS System

To be consistent with our numerical analysis of modes supported by the structure in figure (2.1), we will assume the conductor layer is of the same width as the width of the gap-dielectric-substrate layers. The permittivities used in simulations are $\epsilon_c = -15.822 + 1.075i$ [22], $\epsilon_d = 3.13$, $\epsilon_s = 2.1$ and $\epsilon_g = 1.0$ for Ag, SiO₂-TiO₂, SiO₂ and air at $\lambda = 632.8$ nm respectively.

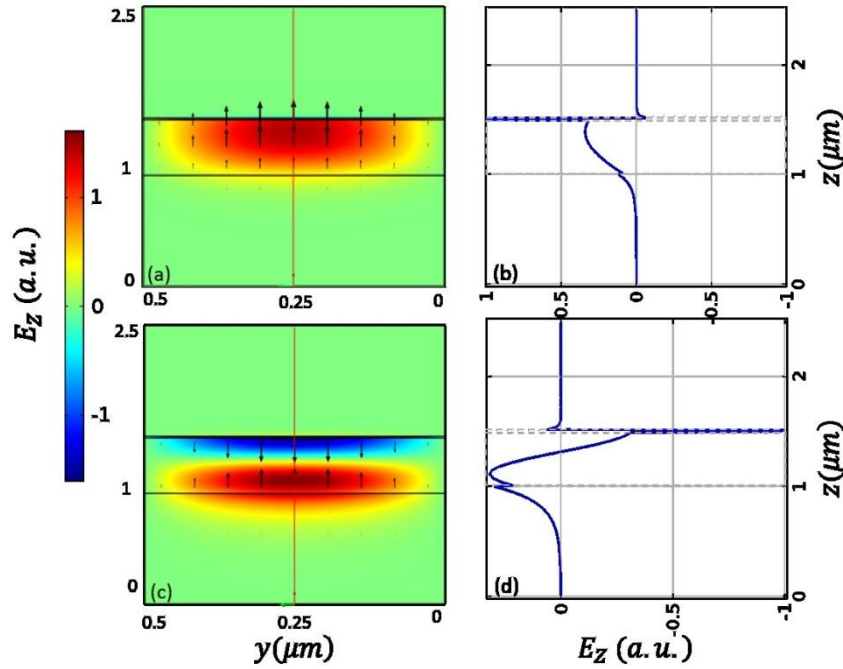


Figure 3.1: Electric field component of (a) the TM-quasi-even and (c) the TM-quasi-odd modes supported by the hybrid coupler. (b) and (d) are corresponding electric field at $y=0.25$ μm in the y - z plane.

To guarantee a good coupling between the two waveguides, the following structural parameters are selected in the simulation: $w_d = 500$ nm, $t_d = 500$ nm, $t_s = 760$ nm, $w_c = 500$ nm, $t_c = 304$ nm, and $t_g = 17$ nm. Figures (3.1a) and (3.1c) depict the

electric field component E_z of the two supermodes supported by the structure at $t_g = 17$ nm. Red line in figures. (3.1a) and (3.1c) at $y = 0.25 \mu\text{m}$ corresponds to the middle of the structure. Figures (3.1b) and (3.1d) provide the E_z profile at $y = 0.25 \mu\text{m}$ for the TM-quasi-even and the TM-quasi-odd modes. It can be seen that for the TM-quasi-even mode, the electric field directions in the gap and in the film are the same while they are opposite in the TM-quasi-odd mode, as shown by black arrows.

3.2 Field Exchange in the CGDS System

Figure (3.2a) provides the light intensity profile in the $x-z$ plane for $y = 0.25 \mu\text{m}$ as a function of the position x when the dielectric mode is excited first at $x = 0$. In the COMSOL model, this is achieved by a simple excitation of the two supermodes with appropriate relative phases. As x increases, the field transfers from the dielectric waveguide to the gap plasmonic waveguide gradually owing to the interference of the TM-quasi-even and TM-quasi-odd eigenmodes.

At a distance x equal to the coupling length L_c , almost all the fields transfer to the gap mode, then the field transfers back to the film mode at $x = 2L_c$. The coupling length $2.1 \mu\text{m}$ found from equation (2.19) matches well the Comsol results as depicted in figure (2.2) from the previous chapter. Figure (3.2b) depicts periodic energy exchange along the propagation length x (light intensity in the gap at the surface of the film). Graduate decrease of energy from one period to another is consistent with $19.92 \mu\text{m}$ propagation length calculated from equation (2.18).

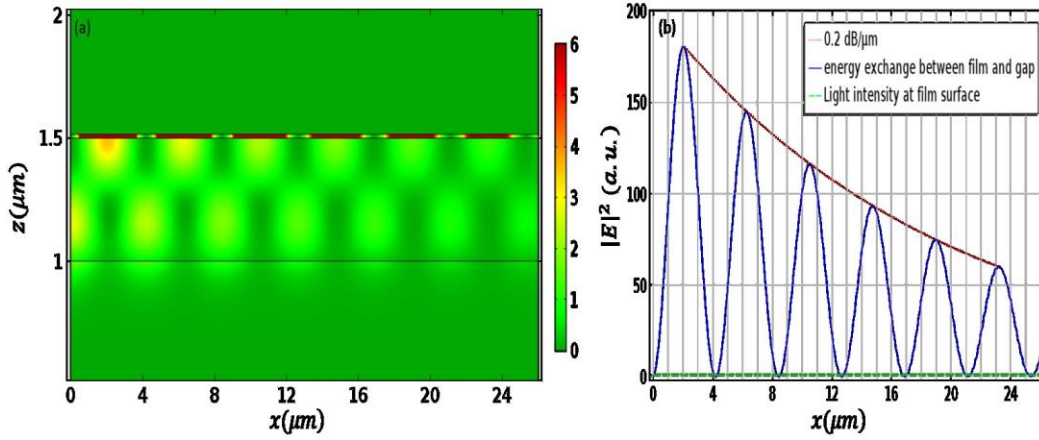


Figure 3.2: (a) Light intensity profile along x - z plane corresponds to $y = 0.25 \mu\text{m}$. (b) Periodic energy exchange along the propagation length x .

The dotted line in figure (3.2b) shows exponential decay of intensity corresponding to the loss factor of $0.2 \text{ dB}/\mu\text{m}$ which can be evaluated from equation (2.18). The dashed line shows the level of light intensity at the surface of the dielectric film waveguide in absence of the metal tip. For local field enhancement concept, only one period is needed to illustrate the light intensity exchange from the dielectric film to the nano-gap and then back to the film.

3.3 3-D Version of the CGDS System

Figure (3.3) shows a plot for the 3-D version of the structure previously analyzed in chapter 2. In addition to the variables t_g (gap size) and t_d (film thickness) introduced earlier, figure (3.3) shows other dimensions: t_s (substrate thickness), w_d (width of the dielectric film and substrate), w_c (width of the conductor). The following structural parameters are selected in the simulation: $w_d = 500 \text{ nm}$, $t_d = 500 \text{ nm}$, $t_s = 760 \text{ nm}$, $w_c = 200 \text{ nm}$, $t_c = 304 \text{ nm}$, and $t_g = 17 \text{ nm}$. In Comsol, Perfect Electric Conductor

boundary conditions (PEC) are applied to all boundaries and an extremely fine free triangular meshing is applied to the whole structure.

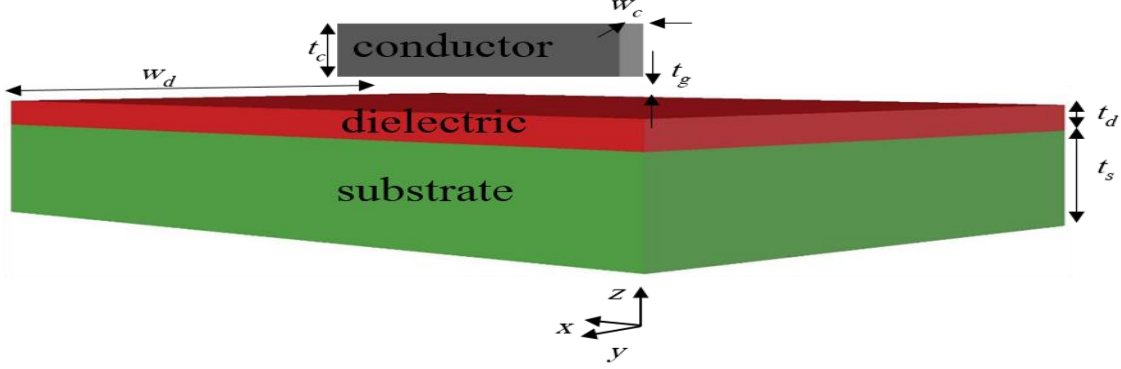


Figure 3.3: Schematic diagram of the hybrid directional coupler. The green region denotes SiO_2 , the red region denotes $(\text{SiO}_2\text{-TiO}_2)$, and the gray region denotes Ag. x is the light propagation direction.

The conductor (metal blade) is physically detached from the rest of the structure. It can be placed at the desirable location using AFM-style nano-positioners. The proposed system thus belongs to the category of tip-enhanced tools [52], which provides local, on demand, enhancement of the electromagnetic field at the location of this specially designed tip.

Figures (3.4a) and (3.4b) depict the electric field component E_z of the silica-titania dielectric mode at $x = 0$ and the corresponding E_z profile at $y = 0.25 \mu\text{m}$. The simulation figures are obtained from the finite-element-method based commercial software Comsol Multiphysics. The obtained modal index n^* for the fundamental ($m = 0$) silica-titania dielectric mode is 1.685 at 632.8 nm. This value is slightly less compared to the modal index evaluated theoretically from equation (2.10) at $t_g \rightarrow \infty$. The reason for this difference is the lateral confinement (finite size in the y -direction) in the Comsol model.

3.4 Comparison Between Before and After Adding Conductor Layer

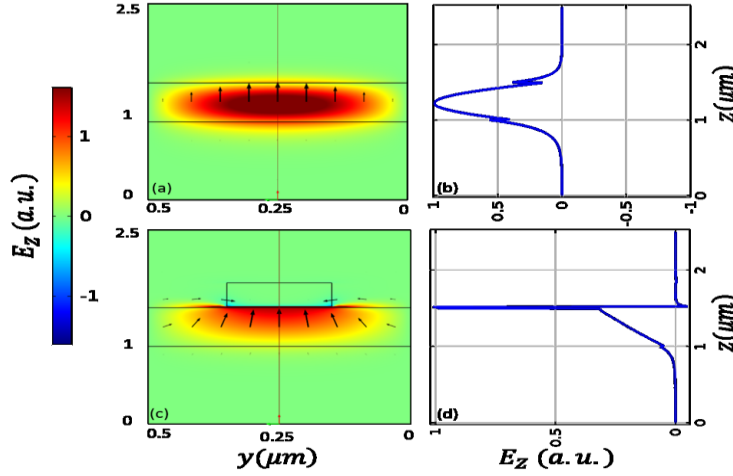


Figure 3.4: Electric field component E_z of (a) The silica-titania dielectric mode in the y - z plane. (b) The corresponding E_z profile at $y = 0.25$ μm along $x = 0$. (c) Electric field component E_z of the coupled mode at $t_g = 17$ nm and (d) The corresponding electric field E_z profile at $y = 0.25$ μm along $x = 0$.

As soon as the silver blade is approaching the top of the structure to form what we call CGDS system, the film mode couples to the plasmonic mode supported by the bottom surface of the silver blade.

Figures (3.4c) and (3.4d) depict the electric field component E_z of the coupled modes at $x = 0$ along the y - z plane, and the corresponding E_z profile at $y = 0.25$ μm respectively. It is apparent that as soon as the silver blade reached the film surface but separated from it by a gap thickness 17nm, the mode mostly confines tightly in the gap than in the film. This behavior explains the field enhancement in the nano-scale gap layer.

3.5 Local Field Enhancement in the CGDS Structure

Although the concept of energy exchange is well illustrated by the interaction between the two guided modes in section (3.2), it does not account for scattering in the CGDS structure with finite dimensions of the conductor tip. Below we consider the thin film mode ($m = 0$) launched at $x = 0$, while the $4.2 \mu\text{m}$ wide tip is centered at $x = 17.1 \mu\text{m}$. This film mode has a modal index $n^* = 1.685$ as was mentioned earlier in the text. It propagates freely in the film and once it reaches the metal tip, it interacts with the CGDS structure. Not only it couples with the gap mode, but it also scatters in all possible directions owing to the sharp corners of the metal tip.

Figure (3.5a) depicts the relative intensity of light in the $x - z$ plane for $y = 0.25 \mu\text{m}$ as a function of the position x when the thin film mode ($m = 0$) is launched at $x = 0$. Figure (3.5 b) depicts the local light intensity in the $x - z$ plane at $z = 1.5 \mu\text{m}$. It is obvious that the intensity in the gap is more than one order of magnitude stronger than at the film surface. This is what we refer to as local field enhancement on demand in the CGDS structure.

The interference of guided modes propagating in the waveguide forward and backward results in periodical variations in intensity with period equals to $\lambda / 2n^* \approx 0.2 \mu\text{m}$. Periodicity of intensity pattern is visible in Figures (3.5a) and (3.5b). Figure (3.5b) shows a small depth of intensity modulation in the interference pattern which indicates weak reflection in the CGDS structure.

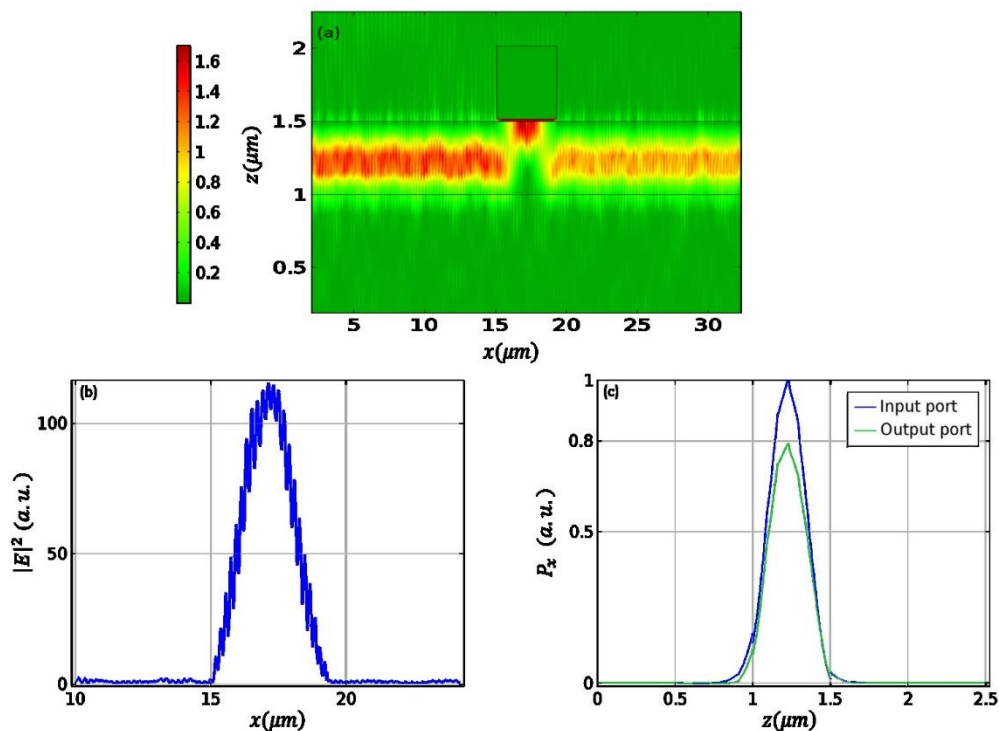


Figure 3.5: (a) Relative intensity of light along $x - z$ plane corresponds to $y = 0.25 \mu\text{m}$. (b) Light intensity in the gap along the propagation length x . (c) Power flux for the dielectric film mode at the input port ($x = 0 \mu\text{m}$) and at the output port ($x = 34.2 \mu\text{m}$).

Figure (3.5a) shows a drop in the overall intensity level by approximately 1dB. This total attenuation is due to both, absorption in metal and scattering by the metal tip. Attenuation due to absorption in metal while guided mode propagates under $4.2 \mu\text{m}$ wide tip is estimated to be $0.2 \text{ dB}/\mu\text{m} \times 4.2 \mu\text{m} = 0.84 \text{ dB}$. This leaves about 0.16 dB for overall scattering. Interference with other scattered waves results in some distortion in the modal field also visible in figure (3.5b).

Figure (3.5c) shows power flux for the dielectric film mode at the input port ($x = 0 \mu\text{m}$) and at the output port ($x = 34.2 \mu\text{m}$). The units are arbitrary and the power flux for the input and output ports are normalized. The value of the power flux at the output port drops by 1dB is consistent with figure (3.5a). Port boundary conditions are used to

launch the mode into the structure. Perfect Electric Conductor boundary conditions (PEC) are applied to the top and bottom boundaries.

3.6 Multi-Field Enhancement in the CGDS system

Multiple field enhancement in the CGDS system can be achieved by placing multiple metal-tips close to the film surface but separated from the surface by a gap layer. Figure (3.6a) depicts the relative intensity of light in the $x-z$ plane for $y = 0.25 \mu\text{m}$ as a function of the position x when the thin film mode ($m = 0$) is launched at $x = 0$. Figure (3.6b) depicts the multiple local light intensity in the $x-z$ plane at $z = 1.5 \mu\text{m}$. It is evident that the intensity in the first gap is more than one order of magnitude stronger than at the film surface. The intensity in the second and in the third gap decreases gradually owing to the ohmic losses and scattering due to the presence of metal tips. These enhancement under the metal tips are what we refer to as multiple local field enhancement on demand in the CGDS structure.

Figure (3.6c) shows power flux for the dielectric film mode at $x = 9.3 \mu\text{m}$, $x = 19.3 \mu\text{m}$ and $x = 29.3 \mu\text{m}$. The units are arbitrary, and the power flux for the different x -scales are normalized. The power flux for the dielectric film mode at $x = 9.3 \mu\text{m}$ is the same as the output power flux previously discussed in figure (3.5c). Thus, this power flux accounts for almost 80% of the power flux at the input port. Figure (3.6c) shows that at $x = 29.3 \mu\text{m}$, the power flux is approximately 58% of the power flux at $x = 9.3 \mu\text{m}$. Therefore, the output power flux in the multiple field enhanced structure is $0.58 \times 0.8 = 0.46$. This attenuation is translated to 3.37 dB.

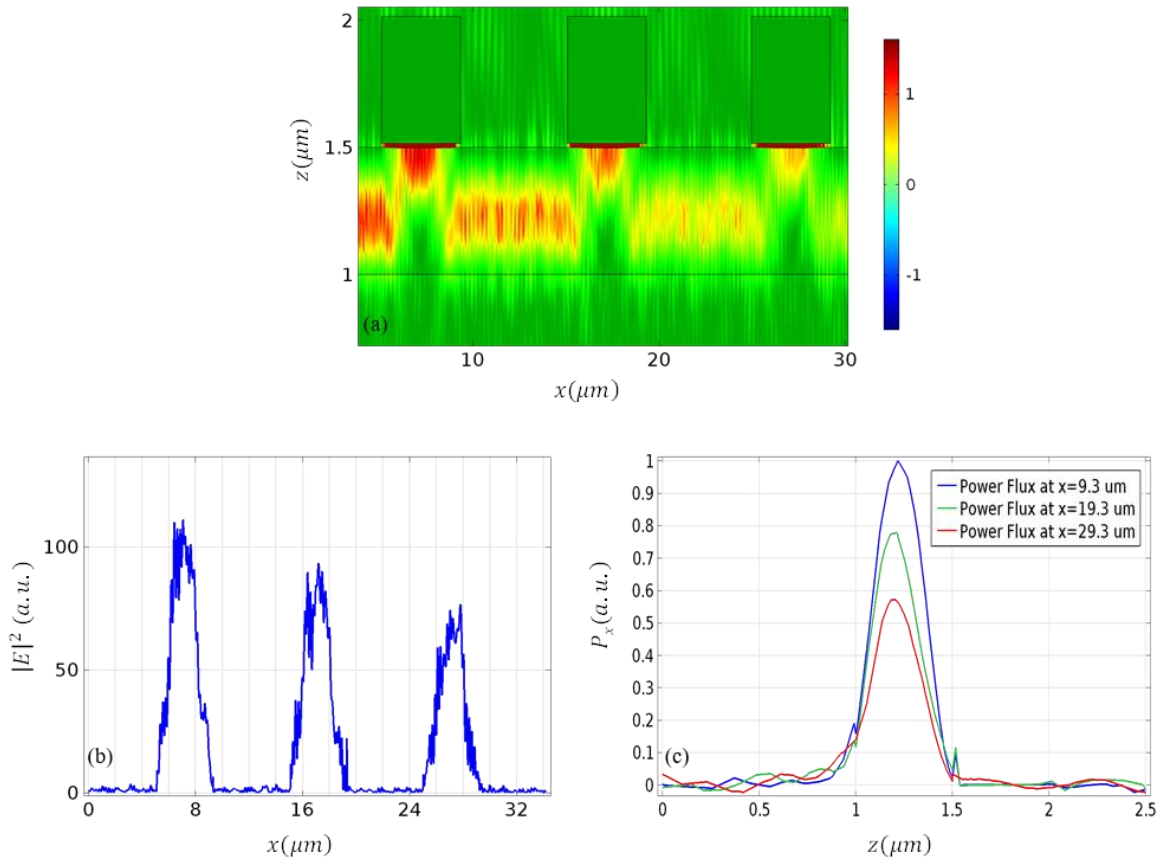


Figure 3.6: (a) Relative intensity of light along $x - z$ plane corresponds to $y = 0.25 \mu\text{m}$. (b) Light intensity in the multiple gaps along the propagation length x . (c) Power flux for the dielectric film mode at $x=9.3 \mu\text{m}$, $x=19.3 \mu\text{m}$, and $x=29 \mu\text{m}$.

This concludes that figures (3.6a) and (3.6c) show a drop in the overall intensity level by approximately 3.37dB. This total attenuation is due to both, absorption in metal and scattering by the metal tip. Attenuation due to absorption in metal while guided mode propagates under $4.2 \times 3 = 12.6 \mu\text{m}$ wide tips is estimated to be $0.2 \text{ dB}/\mu\text{m} \times 4.2 \mu\text{m} \times 3 = 2.52 \text{ dB}$. This leaves about 0.85 dB for overall scattering. Interference with other scattered waves results in some distortion in the modal field also visible in figure (3.6b).

3.7 Conclusion

Local field enhancement on demand based on vertical directional coupling between film mode and gap plasmonic mode in the CGDS has been proposed and investigated using a finite element method simulations. The structure provides strong on-demand field enhancement at the surface of the dielectric film waveguide. Multiple field enhancement in the CGDS system is also presented. Such a hybrid structure can be potentially exploited for developing photonic-plasmonic hybrid functional components for signal routing, power splitting, etc. in PICs. This structure is well suitable for applications which require light-matter enhanced interactions. In particular, it is very useful for biomedical applications where the visible range of wavelength is used.

CHAPTER 4 APPLICATIONS OF THE CONDUCTOR-GAP-DIELECTRIC-SUBSTRATE SYSTEM

4.1 General Applications

Optical devices using a visible spectral range of wavelength have interesting applications in the biomedical field. In this dissertation, we use HeNe laser with a wavelength of 632.8nm located in the red zone among the spectrum. Overall the applications, we consider those which require high light-matter interaction aiming to enhance the interaction between incident photons and nano-scale objects. The task is then to study and analyze the characteristics of these nanoparticles regarding of their absorption/emission characteristics. Such nano-scale dimension particles in the biomedical study can be for example but not limited to DNA, Chromosome, nano-scale tumor tissue or artificial nano-scale objects like Quantum dots.

4.2 Possible System

The system is an on-chip optical spectrometer that would ultimately measure absorption/emission spectra of individual quantum objects or similar objects, such as large molecules or quantum dots [53].

This dissertation aims to enhance the overall system efficiency and hence improve the light-matter interaction. The overall work is a theoretical study integrated with numerical simulations based on finite-element method from Comsol Multiphysics to simulate an on-demand plasmonic-dielectric hybrid coupler. The focused beam is incident on silica-titania ($\text{SiO}_2\text{-TiO}_2$) planar multi-mode waveguide. The waveguide is intentionally made of transparent material to fit biomedical optics applications.

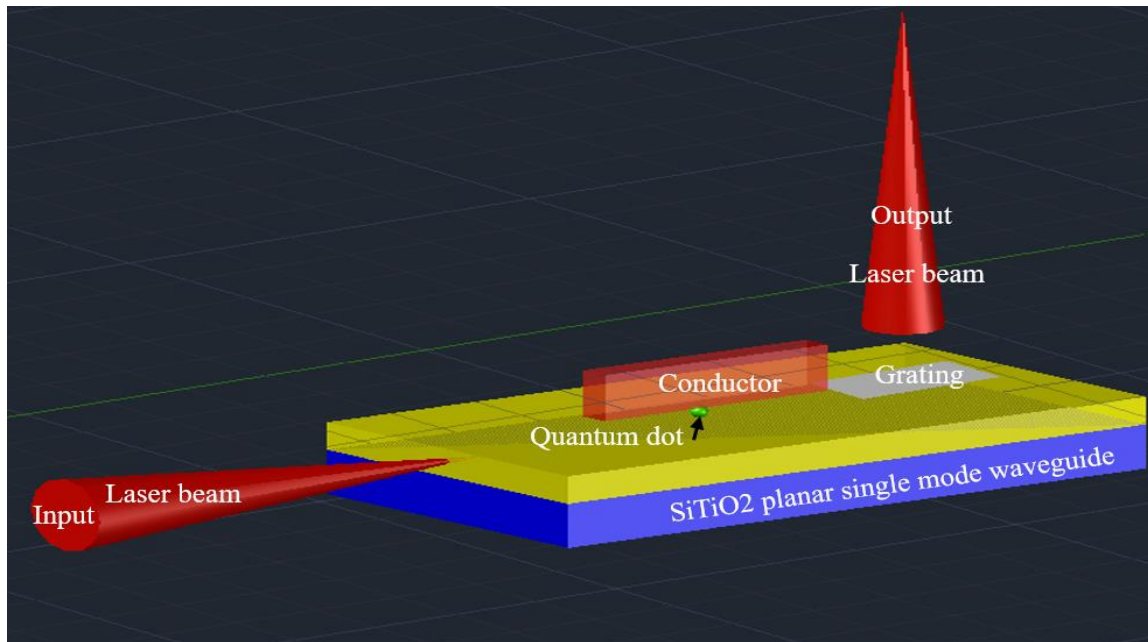


Figure 4.1: Concept of an integrated optical device for the spectroscopy of a single molecule using local field enhancement based on hybrid plasmonic-dielectric waveguide directional coupler.

Figure (4.1) shows the schematic diagram of a possible system. Light is first guided by a planar waveguide but when a tip-enhanced metal is aligned vertically on the top of the $\text{SiO}_2\text{-TiO}_2$ waveguide but separated from it by a gap of a nano-scale dimension, the energy transfers to the nano-gap. After traveling a distance of several micrometers, light energy is transferred back into dielectric mode. The coupling length should not exceed a fraction of the decoupled plasmonic propagation length to avoid high ohmic losses. The dielectric mode propagates to the end of the planar waveguide where a grating is placed to reflect the energy of light to be then captured by a sensor. A rich information about emission-absorption spectra of an individual quantum dot (QD) or a similar object can be obtained due to a highly enhanced field in the gap. For such a system to work appropriately; light intensity coupled back to the dielectric mode has to be over 50% of its original value. Different materials and structure arrangements

of the hybrid directional coupler could be realized for the use in different applications. For instance, conductor can have various shapes. Possible shapes of the conductor layer can be, for instance, a blade, a wedge, or a cone shape. The cone and wedge shapes can be chosen to provide a variable gap length for the plasmonic mode to enable the study of a periodic energy exchange in the hybrid coupler. Also, a conductor with a curved surface to provide a variable gap thickness can be used.

The layers in the CGDS system can be made of different materials (different modal indices). Different materials will have a different impact on the CGDS system performance regarding mode confinement and coupling. However, our choice was to work with transparent materials like silica and silica-titania as they are used to fabricate the hybrid waveguides (microscope samples in the biomedical field applications).

The CGDS system is also compatible to operate at other wavelength scales than the HeNe laser (632.8nm). In fact, the impact might be higher for technically more relevant wavelengths, like 1550 nm used in telecommunications or the commonly used Raman excitation wavelengths of 532 nm or 780 nm. For instance, it is more suitable to use the green laser (532nm) as the input power source when studying the absorption/emission spectra for artificial nano-scale objects like quantum dots. Quantum dots strongly absorb the green laser and emit the red light [54]. One need to pay attention that changing the operating wavelength or materials will require tuning to the physical parameters to optimize the structure so that it works efficiently. In this dissertation, our choice was to use a visible red light (632.8nm) as it is more suitable for the applications in the biomedical field.

4.3 Advantages of Field Enhancement Of the CGDS Plasmonic Mode Over Other Techniques

Light-matter interaction in nanometer-scale size is a very interesting topic in the visible wavelength range [55]. Field enhancement due to optical resonators has been extensively studied. Among different proposal structures, the two-dimensional photonic crystal cavities are found to be the most desirable configuration as they are the best in terms of controlling optical properties. Quantum dots have shown an extreme brightness when they are resonant with photonic crystal cavity mode [55, 56]. However, these studies indicate that the spectroscopy can only be done at only an extremely narrow spectral window about the designed resonant wavelength. Because intensities of the nonresonant photons are significantly small, quantum dots spectra analysis is limited to the resonance of the cavity. The CGDS plasmonic-dielectric hybrid coupler breaks this limitation. The reason is that the field enhancement is not due to the cavity resonance rather it is due to CGDS plasmonic mode. Hence, a study of emission-absorption spectra of quantum dots can be displayed on a large scale of the wavelength.

4.4 Conclusion

CGDS system may be a basic block component to be integrated into various optical or optoelectronic devices. The system can operate in visible as well as in invisible range of the wavelength spectrum. The different wavelength or different structure materials will highly affect the performance of the device. Therefore, to efficiently design the CGDS system, one need to sweep its physical parameters and wavelength to get to the optimal system performance.

CHAPTER 5 COMPREHENSIVE ANALYSIS OF THE DISPERSION EQUATION OF THE CGDS SYSTEM

5.1 Guided Modes in CGDS with Film Thickness in a Micro-Meter Scale

Figure (5.1) shows the CGDS system consisting of all basic structures. Guided modes in the two-layer (conductor-dielectric) and three-layer (conductor-gap-dielectric) systems exist in the four-layer (conductor-gap-dielectric-substrate) system. Thus; the CGDS system is considered a comprehensive system. The study of the CGDS dispersion relation reveals all the information about the guided modes in the two-layer and three-layer systems.

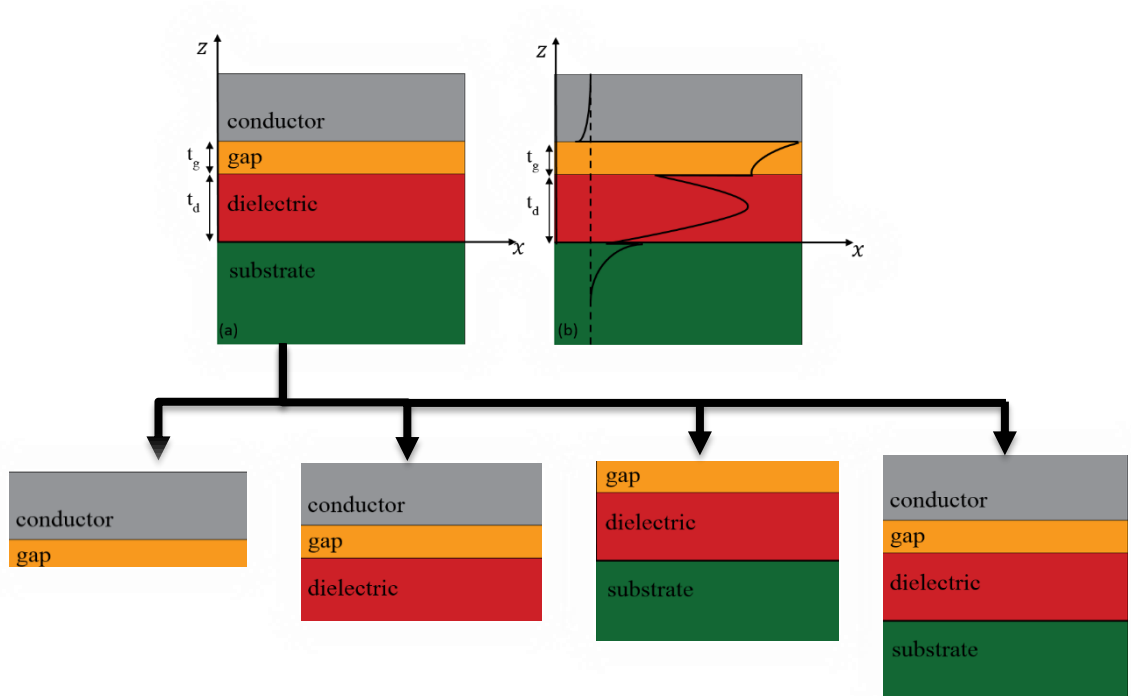


Figure 5.1: Structure of the CGDS system composed of all basic structures.

It should be mentioned that the thicker the dielectric film, the more guided modes carried by the system. In chapter 2, we found that the 500 nm dielectric film thickness can carry only two guided modes, the fundamental ($m = 0$) and the first order ($m = 1$) modes. In this chapter, we will consider a more general case, in which a thicker dielectric film is to be used in the dispersion relation analysis of the CGDS system. The aim of studying the dispersion relation for such a system is to have a better understanding of all possible guided modes in the structure. For instance, a $2\mu\text{m}$ film thickness will now allow six guided modes in the dielectric film. We can name them as follows: the fundamental ($m = 0$), the first order ($m = 1$), the second order ($m = 2$), the third order ($m = 3$), the fourth order ($m = 4$), and fifth order ($m = 5$) mode. The solution of the dispersion equation reveals all possible guided modes in the CGDS system. Guided modes in the CGDS system can be divided as follows:

1. Surface Plasmon Polariton (SPP) guided mode: this mode exists when the gap layer thickness is very small, less than 0.1 nm. In this case, the CGDS system converges to a three-layer (conductor-dielectric-substrate) system. SPP mode exists at the conductor-dielectric interface will have effective modal index larger than the modal index of the dielectric film, i.e. $n_{SPP}^* > n_d$.
2. Gap guided modes: these guided modes exist when the gap layer is larger than 0.1 nm. To be specific, when the gap size is between 10nm-100nm, the low-index gap layer can highly confine such modes. These modes originally exist in the three-layer (conductor-gap-dielectric) system. However, in the CGDS system, the presence of the substrate layer allows the high-index dielectric film to confine and

guide its own mode simultaneously with the gap mode guided by the low-index gap layer.

3. Thin film guided mode: As the gap size gets larger than 100nm, the low-index gap is no longer able to confine and guide modes. The dielectric film will be dominant in this case. Thin film guided modes will have effective modal indices larger than the modal index of the substrate layer but smaller than the modal index of the dielectric layer. i.e $n_s < n^* < n_d$.
4. The leaky modes: As the name indicates, these modes are no longer guided modes rather they are leaky. These modes will have effective modal indices smaller than the modal index of the substrate layer. i.e $n^* < n_s$.
5. Fabry-Perot modes: these modes will have effective modal indices smaller than the effective modal index of the two-layer (conductor-gap) system. For instance, using same materials in chapter 3, these modes will have effective modal indices less than 1.03.

5.2 Comparison Between Dispersion Relation in the CGD and CGDS Systems

At a very small gap thickness less than 1nm, a three-layer (conductor-dielectric-substrate) system is so-called Metal-Cladding waveguide. Figure (5.2a) shows a surface plot for the dispersion relation in the Metal-Cladding waveguide. Figure (5.2b) depicts all possible guided modes in the system. With a 2 μm film thickness, this system supports six modes as shown in figure (5.2b). At a very large gap thickness larger than 1 μm , a three-layer (dielectric-gap-substrate) system is so-called Thin-Film waveguide

system. Figure (5.3a) shows a surface plot for the dispersion relation in the Thin-Film waveguide system. (5.3b) depicts all possible guided modes in the system. With a $2\mu\text{m}$ film thickness, this system supports seven modes as shown in figure (5.3b). Appendix A is provided at the end of this dissertation. It contains a Matlab script to plot the dispersion relation for the Metal-Cladding and for the Thin-Film waveguides.

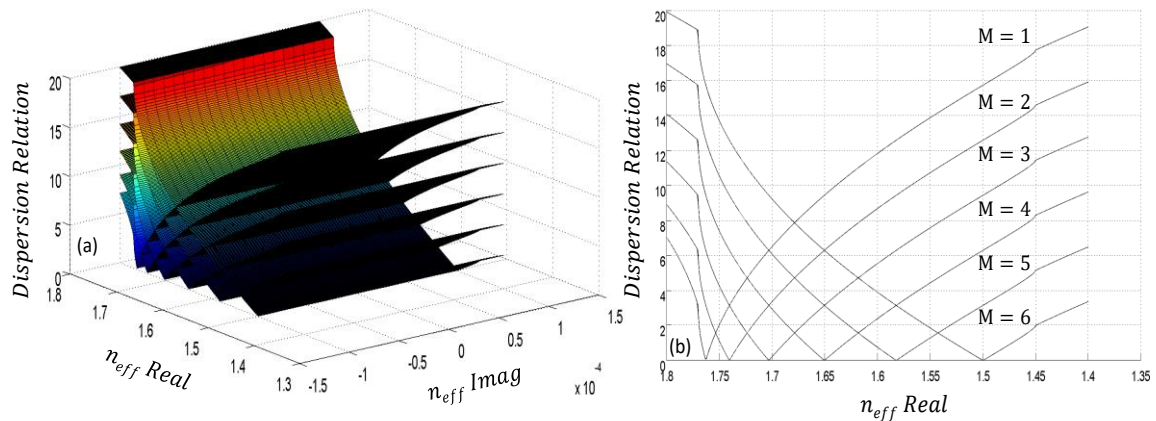


Figure 5.2: (a) Dispersion relation surface plot for the Metal-Cladding waveguide. (b) Modes in the Metal-Cladding waveguide with dielectric layer thickness of $2\mu\text{m}$.

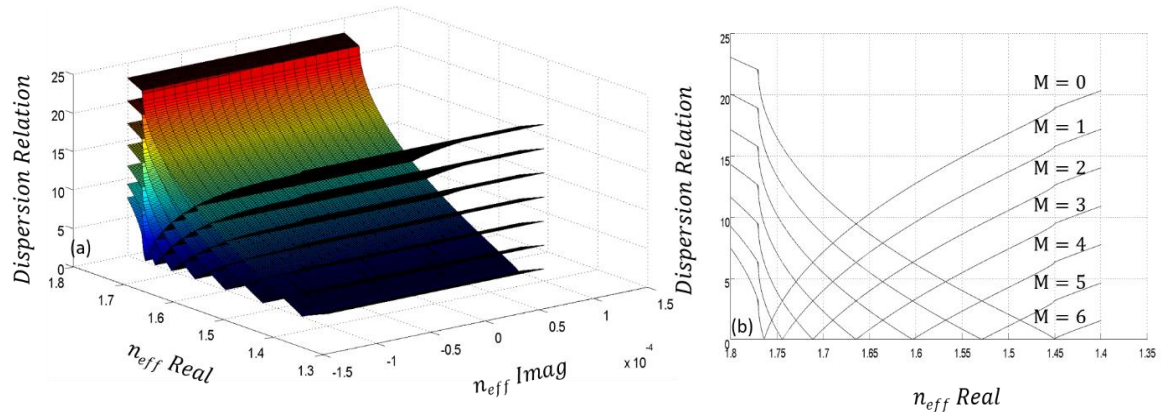


Figure 5.3: (a) Dispersion relation surface plot for the Thin-Film waveguide. (b) Modes in the Thin-Film waveguide with dielectric layer thickness of $2\mu\text{m}$.

Figure (5.4) shows some of the possible solutions (modes) of the dispersion equation in the CGDS system with film thickness of $2\mu\text{m}$. These modes are: Plasmonic

modes, Metal-Cladding waveguide modes, hybrid modes and Thin-Film waveguide modes. For instance, the mode 1.971 at $t_g = 10^{-4}$ μm is the plasmonic mode of the two-layer (conductor-dielectric) system which can be calculated using:

$$n_{spp} = \sqrt{\frac{\epsilon_d \times \epsilon_c}{\epsilon_d + \epsilon_c}} \quad (5.1)$$

The mode 1.033 at $t_g = 10$ μm is the plasmonic mode of the two-layer (conductor-gap) system which can be obtained using:

$$n_{spp} = \sqrt{\frac{\epsilon_g \times \epsilon_c}{\epsilon_g + \epsilon_c}} \quad (5.2)$$

As we are not showing all the solutions of the dispersion relation for the CGDS system, we only show the first plasmonic mode 1.971 at $t_g = 10^{-4}$ μm in figure (5.4).

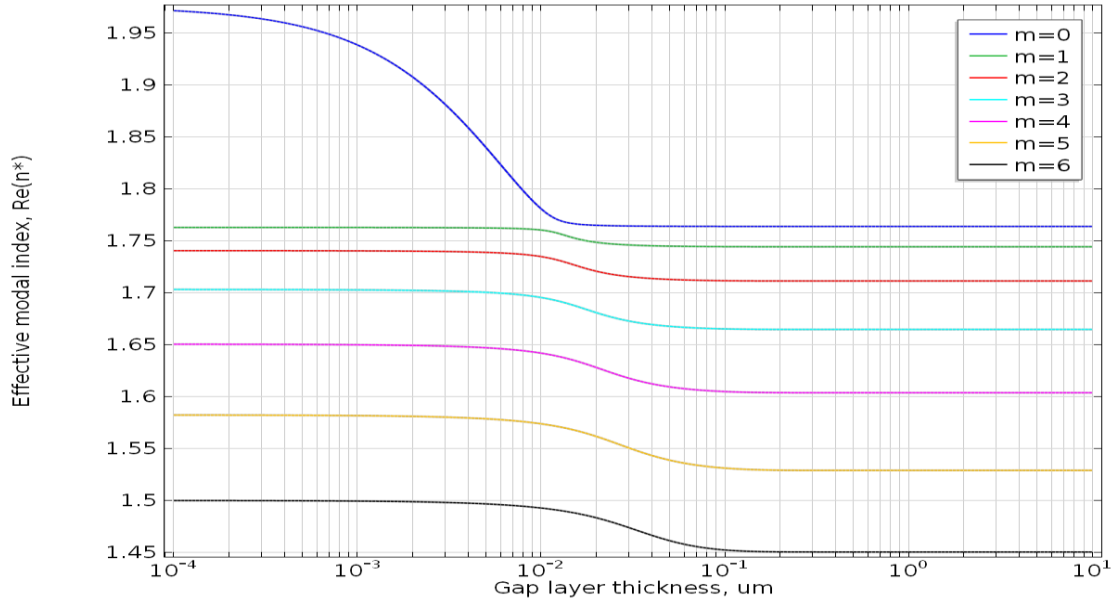


Figure. 5.4: Modal indices of guided modes versus gap thickness, materials from top to bottom are Ag, air, SiO₂-TiO₂, and SiO₂ at $\lambda = 632.8$ nm respectively. Film thickness= $2\mu\text{m}$.

Comparing figures (5.2b) and (5.3b) with the figure (5.4), one can find that the modal indices of the CGDS system at $t_g = 10^{-4}$ are the modal indices for the Metal-Cladding waveguide with a dielectric layer thickness of 2 μm . Also, the modal indices of the CGDS system at 10 μm are the modal indices for the Thin-Film waveguide with a dielectric layer thickness of 2 μm .

5.3 Electromagnetic Field Analysis and Simulation in the CGDS System

The aim of this section is to plot the electric and magnetic field profiles at any value of the effective modal index on the dispersion relation graph. The goal is to have a complete picture of how the field's distributions for the guided modes look like in the CGDS system. To generate such plots, we can start with magnetic field H_y equations, solve for the constants then running a Matlab code to generate the field's graphs. The magnetic field equations to be used here are taken from chapter 2:

$$H_y(x, z) = Fe^{sz}e^{ik_x \cdot x}, \quad \text{if } z < 0. \quad (5.3)$$

$$H_y(x, z) = [De^{(pz)} + Ee^{-(pz)}]e^{ik_x \cdot x}, \quad \text{if } 0 \leq z < t_d. \quad (5.4)$$

$$H_y(x, z) = [Be^{q(z-t_d)} + Ce^{-q(z-t_d)}]e^{ik_x \cdot x}, \quad \text{if } t_d \leq z \leq t_g + t_d. \quad (5.5)$$

$$H_y(x, z) = Ae^{-r(z-t_g-t_d)}e^{ik_x \cdot x}, \quad \text{if } z \geq t_g + t_d. \quad (5.6)$$

Where A, B, C, D, E and F are constants. To find the constants we can assume, for instance, that F=1. To find the other constants, match the boundary conditions (H_y is continuous, and derivative of H_y divided by ε is continuous): we have three boundaries here. The first boundary is between the substrate and the dielectric at $z = 0$.

$$H_y(z < 0) = H_y(0 < z < t_d) \quad (5.7)$$

$$H_y(0 < z < t_d) = H_y(t_d < z < t_g + t_d) \quad (5.8)$$

$$H_y(t_d < z < t_g + t_d) = H_y(z > t_g + t_d) \quad (5.9)$$

$$\frac{1}{\varepsilon} \frac{\partial H_y}{\partial z}(z < 0) = \frac{1}{\varepsilon} \frac{\partial H_y}{\partial z}(0 < z < t_d) \quad (5.10)$$

$$\frac{1}{\varepsilon} \frac{\partial H_y}{\partial z}(0 < z < t_d) = \frac{1}{\varepsilon} \frac{\partial H_y}{\partial z}(t_d < z < t_g + t_d) \quad (5.11)$$

$$\frac{1}{\varepsilon} \frac{\partial H_y}{\partial z}(t_d < z < t_g + t_d) = \frac{1}{\varepsilon} \frac{\partial H_y}{\partial z}(z > t_g + t_d). \quad (5.12)$$

Substituting in equations (5.7) and (5.10), the first boundary is at $z = 0$:

$$F e^{sz} = D e^{(pz)} + E e^{-(pz)}, \quad (5.13)$$

$$\frac{s}{\varepsilon_s} F e^{sz} = \frac{p}{\varepsilon_d} [D e^{(pz)} - E e^{-(pz)}], \quad (5.14)$$

substitute $F=1$, and $z=0$ in equations (5.13) and (5.14), one can get:

$$1 = D + E, \quad (5.15)$$

$$\frac{s}{\varepsilon_s} \frac{\varepsilon_d}{p} = D - E, \quad (5.16)$$

solving equations (5.15) with (5.16), one can find D and E as follows:

$$E = \frac{1}{2} \left[1 - \frac{s}{\varepsilon_s} \frac{\varepsilon_d}{p} \right], \quad (5.17)$$

$$D = 1 - \frac{1}{2} \left[1 - \frac{s}{\varepsilon_s} \frac{\varepsilon_d}{p} \right]. \quad (5.18)$$

Substituting in equations (5.8) and (5.11). The second boundary is between the dielectric and the gap layers at $z = t_d$.

$$De^{(pt_d)} + Ee^{-(pt_d)} = B + C \quad (5.19)$$

$$\frac{p}{\epsilon_d} [De^{(pt_d)} - Ee^{-(pt_d)}] = \frac{q}{\epsilon_g} [B - C] \quad (5.20)$$

Solving equations (5.19) with (5.20) with definitions of D and E from equations (5.17) and (5.18), one can find B and C as follows:

$$B = \frac{1}{2} \left[De^{(pt_d)} \left(1 + \frac{p}{q} \frac{\epsilon_g}{\epsilon_d} \right) + Ee^{-(pt_d)} \left(1 - \frac{p}{q} \frac{\epsilon_g}{\epsilon_d} \right) \right] \quad (5.21)$$

$$C = \frac{1}{2} \left[De^{(pt_d)} \left(1 - \frac{p}{q} \frac{\epsilon_g}{\epsilon_d} \right) + Ee^{-(pt_d)} \left(1 + \frac{p}{q} \frac{\epsilon_g}{\epsilon_d} \right) \right] \quad (5.22)$$

Substituting in equations (5.9) and (5.12). The third boundary is between the gap and the conductor layers at $z = t_d + t_g$.

$$Be^{qt_g} + Ce^{-qt_g} = A \quad (5.23)$$

$$\frac{q}{\epsilon_g} [Be^{qt_g} - Ce^{-qt_g}] = \frac{-r}{\epsilon_c} A \quad (5.24)$$

The constant A can be obtained from either equation (5.23) or (5.24). A Matlab code available in Appendix B is used to plot the field strengths for any effective modal index value in the CGDS system.

Figure (5.5) depict the field strengths for the fundamental ($m = 0$) mode. Figures (5.5a) and (5.5b) shows field strengths at gap thickness $t_g = 10^{-4} \mu\text{m}$ and $n_1^* = 1.971$. This mode is a surface plasmon polariton (SPP) mode. Figures (5.5c) and (5.5d) depict

the field strengths at $t_g = 0.017 \mu\text{m}$ and $n_1^* = 1.764$. This mode is called a Hybrid mode.

Figures (5.5e) and (5.5f) depict the field strengths at $t_g = 10 \mu\text{m}$ and $n_1^* = 1.764$. This mode is called a Thin-Film waveguide mode.

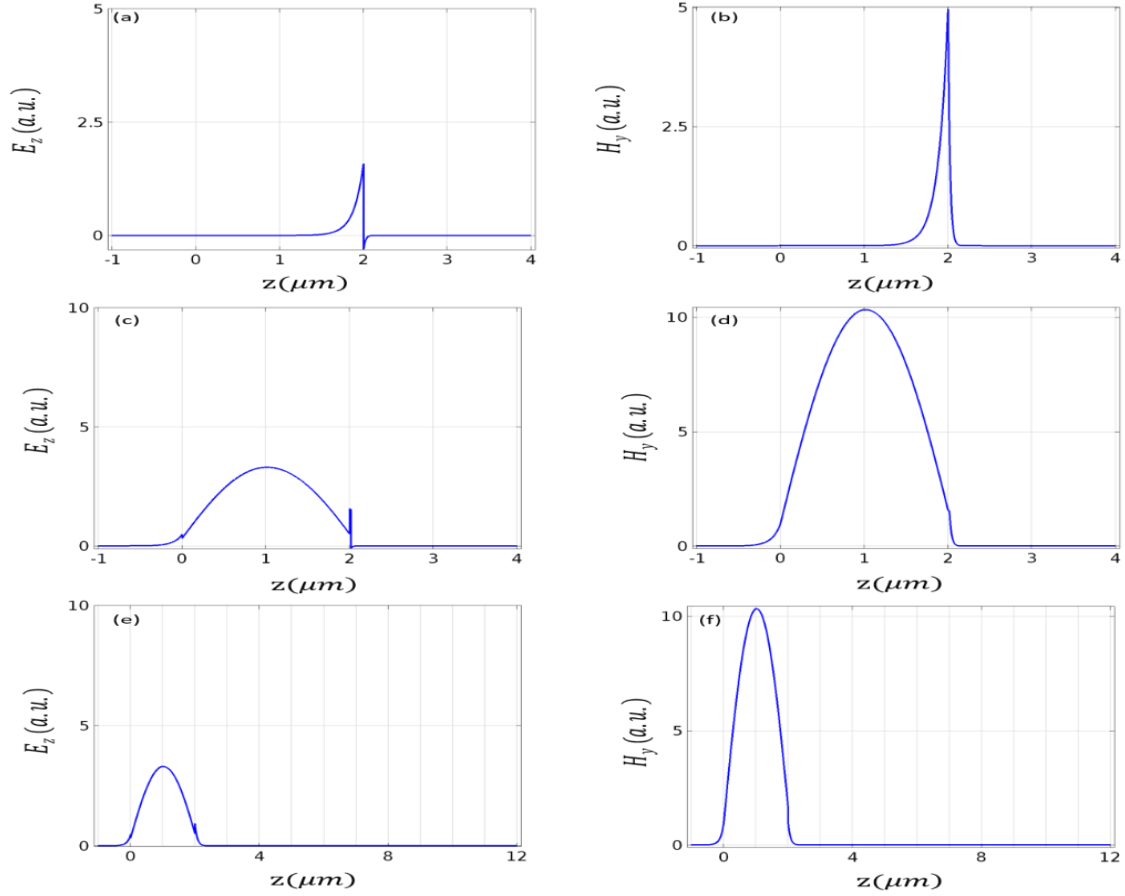


Figure 5.5: Field Strength, a.u. for the fundamental ($m=0$) mode. (a) and (b) : $t_g = 10^{-4} \mu\text{m}$ for $n_1^* = 1.971$. (c) and (d) : $t_g = 0.017 \mu\text{m}$ for $n_1^* = 1.764$ and (e) and (f) : $t_g = 10 \mu\text{m}$ for $n_1^* = 1.764$.

Figure (5.6) depict the field strengths for the first order ($m = 1$) mode. Figures (5.6a) and (5.6b) are the field strengths at gap thickness $t_g = 10^{-4} \mu\text{m}$ and $n_1^* = 1.763$. Figures (5.6c) and (5.6d) depict the field strengths at $t_g = 0.017 \mu\text{m}$ and $n_1^* = 1.744$ and

figures (5.6e) and (5.6f) depict the field strengths at $t_g = 10 \mu\text{m}$ and $n_1^* = 1.744$ respectively.

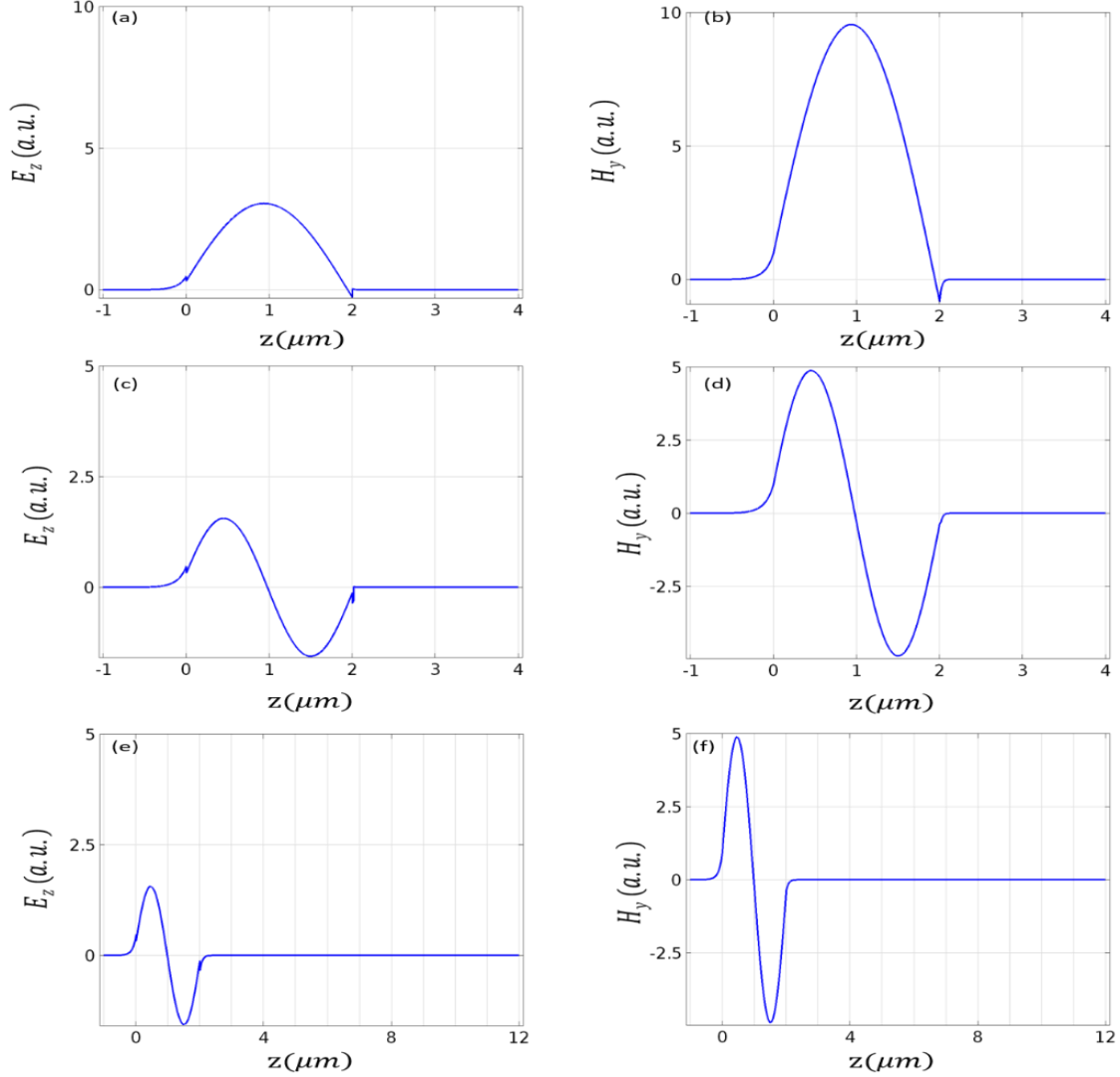


Figure 5.6: Field Strength, a.u. for the first order ($m=l$) mode. (a) and (b): $t_g = 10^{-4} \mu\text{m}$ for $n_1^* = 1.763$. (c) and (d): $t_g = 0.017 \mu\text{m}$ for $n_1^* = 1.744$ and (e) and (f): $t_g = 10 \mu\text{m}$ for $n_1^* = 1.744$.

5.4 Conclusion

CGDS system is a comprehensive system that can confine and guide all possible modes that already exist in lower order (CD and CGD) systems. Dispersion relation

provides the complete picture for all possible guided modes in the CGDS structure. The anti-crossing behavior of guided modes is used to determine the optimal gap layer thickness and hence to obtain the strongest coupling between any two supermodes. Electromagnetic field distributions for various types of guided modes are depicted. Although we have only shown the field strengths for the first two modes, one can use the Matlab code in Appendix B to plot the field strengths for higher order guided modes in the CGDS system. A Mathcad software (as of my choice) is used to plot the dispersion relation of the CGDS system depicted in figure (5.4).

CHAPTER 6 CONCLUSION

6.1 Conclusion

Local field enhancement on demand based on the vertical directional coupling between film mode and gap plasmonic mode in conductor-gap-dielectric-substrate (CGDS) system has been proposed and investigated using an analytical model confirmed by finite element method simulations. The dispersion equation has been derived analytically and solved numerically. The structure provides strong on-demand field enhancement at the surface of the dielectric film waveguide. Such a hybrid structure can be potentially exploited for developing photonic-plasmonic hybrid functional components for signal routing, power splitting, etc. in PICs. This structure is well suitable for applications which require light-matter enhanced interactions. In particular, it is very useful for biomedical applications where the visible range of wavelength is used.

APPENDIX A MATLAB SCRIPT TO PLOT THE DISPERSION RELATION FOR THE METAL-CLADDING AND THIN- FILM WAVEGUIDES

```

% MATLAB code to plot the Dispersion relation for the Metal-Cladding
waveguide and for the Thin-Film waveguide as a surface plot in 3-D.

clc

clear all

close all

neffr = [1.4:0.001:1.8];% range of effective modal index
neffi = [-1e-4:1e-6:1e-4];% range of effective modal index
eps_d = 1.77^2; %permittivity of dielectric layer (guiding layer)
eps_s = 1.45^2; %permittivity of substrate layer (lower layer)
eps_c = -15.822+1.075i; % %permittivity of conductor layer (upper
layer)

eps_g = 1;

d = 2;          %dielectric layer thickness

wl = 0.6328; %wavelength

%parameters related to the z-component of the wave vector

for M = 0:10

    for m = 1:length(neffr)

        for n = 1:length(neffi)

            p = (2.*pi./wl).*sqrt( eps_d - (neffr(m) + neffi(n)).^2) ;
            q1 = (2.*pi./wl).*sqrt((neffr(m) + neffi(n)).^2-eps_c);
            qq = (2.*pi./wl).*sqrt((neffr(m) + neffi(n)).^2-eps_g);
            q2 = (2.*pi./wl).*sqrt((neffr(m) + neffi(n)).^2-eps_s);

```

```

        z1(m,n) = p.*d-atan((eps_d.*q1)./(eps_c.*p))-
atan((eps_d.*q2)./(eps_s.*p))- M.*pi;

        z2(m,n) = p.*d-atan((eps_d.*qq)./(eps_g.*p))-
atan((eps_d.*q2)./(eps_s.*p))-M.*pi;

        end

    end

    subplot(1,2,1)

    surf(neffi,neffr,abs(z1))

    ylabel('neff real ')
    xlabel('neff imag')
    zlabel('Dispersion relation')
    title('Metal-Cladding waveguide')

    grid on

    hold on

    subplot(1,2,2)

    surf(neffi,neffr,abs(z2))

    ylabel('neff real ')
    xlabel('neff imag')
    zlabel('Dispersion relation')
    title('Thin-Film waveguide')

    grid on

    hold off

end

hold off

```

APPENDIX B MATLAB SCRIPT TO CALCULATE AND PLOT THE ELECTRIC AND MAGNETIC FIELDS AT ANY VALUE OF MODAL INDICES ON THE DISPERSION RELATION CURVE

```

%Matlab code generated to calculate and to plot the Electric and
Magnetic fields for any effective modal index value on the dispersion
relation curve

clc

clear all

close all

% CGDS parameters%

neff=[1.4:0.001:1.8]; %range of effective modal index

wl=0.6328; %wavelength of He-Ne Laser

td=2; %thickness of dielectric layer

nd=1.77; % modal index of dielectric layer

ns=1.45; %modal index of substrate layer

ng=1; %modal index of gap layer

nc=0.135+3.98i; %modal index of conductor (silver) layer

epss=ns^2; %permittivity of substrate

epsd=nd^2; %permittivity of dielectric

epsg=ng^2; %permittivity of gap

epsc=nc^2; %permittivity of conductor

k0=2*pi/wl; %wave vector of light wave in free space

% Enter effective modal index and gap layer thickness at which you wish
to

% plot the fields

neff = input('Enter the neff value = ');

```

```

tg = input('Enter the gap thickness value in micrometers unit = ');
%related to the z-components of the wavevector%
s=k0*sqrt(neff^2-epss);
p=k0*sqrt(neff^2-epsd);
q=k0*sqrt(neff^2-epsq);
r=k0*sqrt(neff^2-epsr);
%The Amplitudes (constants) of the magnetic field equations H_y(x,z)%
F=1;
E=0.5*(1-(s*epsd/(p*epss)));
D=1-0.5*(1-(s*epsd/(p*epss)));
B=0.5*((D*exp(p*td)*(1+(p*epsq/(q*epsd))))+(E*exp(-p*td)*(1-(p*epsq/(q*epsd)))));
C=0.5*((D*exp(p*td)*(1-(p*epsq/(q*epsd))))+(E*exp(-p*td)*(1+(p*epsq/(q*epsd)))));
A=B*exp(q*tg)+C*exp(-q*tg);
%layers thicknesses from bottom to top;
z=[-1:0.001:4]
%Equations of H_y(x,z) and E_z(x,y) in the layers;
Hy=zeros(size(z))
a=(z<=0)
Hy(a)=F.*exp(s.*z(a));
Ez(a)=(1/epss)*(Hy(a));
a=(z>0 & z<=2)
Hy(a)=D.*exp(p.*z(a))+E.*exp(-p.*z(a));
Ez(a)=(1/epsd)*(Hy(a));
a=(z>2 & z<=(2+tg))
%Hg=C.*exp(-q.*(zg-td)); % at very large tg

```

```
Hy(a)=B.*exp(q.*(z(a)-td))+C.*exp(-q.*(z(a)-td));
Ez(a)=(1/epsg)*(Hy(a));
a=(z>2+tg)
Hy(a)=A.*exp(-r.*(z(a)-tg-td));
Ez(a)=(1/epsc)*(Hy(a));

%plotting field strength

subplot(1,2,1)

plot(z,Ez)

hold on

xlabel('z, um');
ylabel('Ez, a.u');

%title(' Field strength, a.u. ');

grid on

subplot(1,2,2)

plot(z,Hy)

xlabel('z, um');
ylabel('Hy, a.u');

grid on
```

REFERENCES

1. Desiatov, Boris, Ilya Goykhman, and Uriel Levy. "Plasmonic nanofocusing of light in an integrated silicon photonics platform." *Optics express* 19, no. 14 (2011): 13150-13157.
2. Lodahl, Peter, Sahand Mahmoodian, and Søren Stobbe. "Interfacing single photons and single quantum dots with photonic nanostructures." *Reviews of Modern Physics* 87, no. 2 (2015): 347.
3. Yang, Shang-Hua, and Mona Jarrahi. "Enhanced light-matter interaction at nanoscale by utilizing high-aspect-ratio metallic gratings." *Optics letters* 38, no. 18 (2013): 3677-3679.
4. Moerk, Jesper, and Torben R. Nielsen. "Enhancing Light-Matter Interactions in Nanophotonic Structures by Slow Light." In *Laser Science*, p. LThC2. Optical Society of America, 2010.
5. Janisch, Corey, Haomin Song, Chanjing Zhou, Zhong Lin, Ana L. Elías, Dengxin Ji, Mauricio Terrones, Qiaoqiang Gan, and Zhiwen Liu. "MoS₂ Monolayers on Nanocavities: Enhanced Light-Matter Interaction within Atomic Monolayers." In *CLEO: Science and Innovations*, pp. SF2E-2. Optical Society of America, 2016.
6. Zhang, Jianfa, Wei Liu, Zhihong Zhu, Xiaodong Yuan, and Shiqiao Qin. "Strong field enhancement and light-matter interactions with all-dielectric metamaterials based on split bar resonators." *Optics express* 22, no. 25 (2014): 30889-30898.
7. Kern, Johannes, Andreas Trügler, Iris Niehues, Johannes Ewering, Robert Schmidt, Robert Schneider, Sina Najmaei et al. "Nanoantenna-Enhanced Light-Matter Interaction in Atomically Thin WS₂." *ACS Photonics* 2, no. 9 (2015): 1260-1265.
8. Olmon, Robert L., and Markus B. Raschke. "Antenna-load interactions at optical frequencies: impedance matching to quantum systems." *Nanotechnology* 23, no. 44 (2012): 444001.

9. Bharadwaj, Palash, Bradley Deutsch, and Lukas Novotny. "Optical antennas." *Advances in Optics and Photonics* 1, no. 3 (2009): 438-483.
10. Anger, Pascal, Palash Bharadwaj, and Lukas Novotny. "Enhancement and quenching of single-molecule fluorescence." *Physical review letters* 96, no. 11 (2006): 113002.
11. Kühn, Sergei, Ulf Håkanson, Lavinia Rogobete, and Vahid Sandoghdar. "Enhancement of single-molecule fluorescence using a gold nanoparticle as an optical nanoantenna." *Physical review letters* 97, no. 1 (2006): 017402.
12. Li, Jingjing, David Fattal, and Zhiyong Li. "Plasmonic optical antennas on dielectric gratings with high field enhancement for surface enhanced Raman spectroscopy." *Applied Physics Letters* 94, no. 26 (2009): 263114.
13. AA. Lyamkina, K. Schraml, A. Regler, M. Schalk, AK. Bakarov, AI. Toropov, SP. Moshchenko, M. Kaniber. "Monolithically integrated single quantum dots coupled to bowtie nanoantennas," arXiv preprint arXiv: 1603.07093 (2016).
14. Sun, Yuze, and F. Xudong. "Optical ring resonators for biochemical and chemical sensing." *Analytical and bioanalytical chemistry* 399, no. 1 (2011): 205-211.
15. Lodahl, Peter, Sahand Mahmoodian, and Søren Stobbe. "Interfacing single photons and single quantum dots with photonic nanostructures." *Reviews of Modern Physics* 87, no. 2 (2015): 347.
16. J. D. Jackson. *Classical Electrodynamics*. John Wiley & Sons, New York, 1999.
17. Stefan A. Maier. *Plasmonics: Fundamentals and Applications*. Springer, 2007.
18. Chowdhury, Yassin. "Plasmonic Waveguides: Design and Comparative Study." (2011).

19. Barnes, William L. "Surface plasmon–polariton length scales: a route to sub-wavelength optics." *Journal of optics A: pure and applied optics* 8, no. 4 (2006): S87.
20. Raether, Heinz. *Surface plasmons on smooth surfaces*. Springer Berlin Heidelberg, 1988.
21. H. Raether, "Surface Plasmons on Smooth and Rough Surfaces and on Gratings," (Springer, Berlin, 1988).
22. P. B. Johnson and R. W. Christy, "Optical constants of the noble metals," *Phys. Rev. B* 6, 4370–4379 (1972).
23. Huang, Chia-Chien. "Ultra-long-range symmetric plasmonic waveguide for high-density and compact photonic devices." *Optics express* 21, no. 24 (2013): 29544-29557.
24. Cleary, Justin W., William H. Streyer, Nima Nader, Shiva Vangala, Ivan Avrutsky, Bruce Claflin, Joshua Hendrickson et al. "Platinum germanides for mid-and long-wave infrared plasmonics." *Optics express* 23, no. 3 (2015): 3316-3326.
25. Belan, S., S. Vergeles, and P. Vorobev. "Adjustable subwavelength localization in a hybrid plasmonic waveguide." *Optics express* 21, no. 6 (2013): 7427-7438.
26. Zia, Rashid, Jon A. Schuller, Anu Chandran, and Mark L. Brongersma. "Plasmonics: the next chip-scale technology." *Materials today* 9, no. 7 (2006): 20-27.
27. Bozhevolnyi, Sergey I. "Effective-index modeling of channel plasmon polaritons." *Optics express* 14, no. 20 (2006): 9467-9476.
28. Lou, Fei, Daoxin Dai, and Lech Wosinski. "Ultracompact polarization beam splitter based on a dielectric–hybrid plasmonic–dielectric coupler." *Optics letters* 37, no.

- 16 (2012): 3372-3374.
29. Yin, Mei, Qingzhong Deng, Yanping Li, Xingjun Wang, and Hongbin Li. "Compact and broadband mode multiplexer and demultiplexer based on asymmetric plasmonic–dielectric coupling." *Applied optics* 53, no. 27 (2014): 6175-6180.
 30. R. F. Oulton, V. J. Sorger, D. A. Genov, D. F. P. Pile and X. Zhang "A hybrid plasmonic waveguide for sub-wavelength confinement and long-range propagation," *Nature Photonics* **2**, 496–500 (2008).
 31. L. Chen, J. Shakya, and M. Lipson, "Subwavelength confinement in an integrated metal slot waveguide on silicon," *Opt. Lett.* 31, 2133–2135 (2006).
 32. G. Veronis and S. Fan, "Theoretical investigation of compact couplers between dielectric slab waveguides and two-dimensional metal-dielectric-metal plasmonic waveguides," *Opt. Express* 15, 1211–1221 (2007).
 33. Z. Han, A. Y. Elezzabi, and V. Van, "Experimental realization of subwavelength plasmonic slot waveguides on a silicon platform," *Opt. Lett.* 35, 502–504 (2010).
 34. P. Ginzburg, D. Arbel, and M. Orenstein, "Gap plasmon polariton structure for very efficient microscale-to-nanoscale interfacing," *Opt. Lett.* 31, 3288–3290 (2006).
 35. C. Koos, Jacome, C. Poulton, J. Leuthold, and W. Freude, "Nonlinear silicon-on-insulator waveguides for all-optical signal processing," *Opt. Express* 15, 5976–5990(2007).
 36. R. Hao, E. Li and X. Wei, "Two-dimensional light confinement in cross-index-modulation plasmonic waveguides," *Opt. Lett.* 37, 2934–2936 (2012).

37. D. Arbel and M. Orenstein, "Plasmonic modes in W-shaped metal-coated silicon grooves," *Opt. Express* 16, 3114–3119 (2008).
38. Y. Kou, F. Ye, and X. Chen, "Low-loss hybrid plasmonic waveguide for compact and high-efficient photonic integration," *Opt. Express* 19, 11746–11752 (2011).
39. Q. Li, Y. Song, G. Zhou, Y. Su and M. Qiu, "Asymmetric plasmonic-dielectric coupler with short coupling length, high extinction ratio, and low insertion loss," *Opt. Lett.* 35, 3153–3155 (2010).
40. Q. Li and M. Qiu, "Structurally-tolerant vertical directional coupling between metal-insulator-metal plasmonic waveguide and silicon dielectric waveguide," *Opt. Express* 18, 15531–15543 (2010).
41. Y. Huang, S. Zhu, H. Zhang, T. Liow and G. Lo, "CMOS compatible horizontal nanoplasmonic slot waveguides TE-pass polarizer on silicon-on-insulator platform," *Opt. Express* 21, 12790–12796 (2013).
42. C. Chen, L. Pang, C. Tsai, U. Levy and Y. Fainman, "Compact and integrated TM-pass waveguide polarizer," *Opt. Express* 13, 5347–5352 (2005).
43. J. N. Polky, and G. L. Mitchell, "Metal-clad planar dielectric waveguide for integrated optics," *Journal of Optical Society of America* 64, 274–279 (1974).
44. M. Z. Alam, A. JStewart, and Mo Mojahedi, "Theoretical analysis of hybrid plasmonic waveguide," *Selected Topics in IEEE J. Quantum Electron.* 19, 4602008–4602008 (2013).
45. I. Avrutsky, R. Soref, and W. Buchwald, "Sub-wavelength plasmonic modes in a conductor-gap-dielectric system with a nanoscale gap," *Opt. Express* 18, 348–63

- (2010).
46. L. Wei, S. Aldawsari, L. Wing-Ki, B. R. West "Theoretical Analysis of Plasmonic Modes in a Symmetric Conductor-Gap-Dielectric Structure for Nanoscale Confinement," *IEEE Photonics Journal* 6, 1–10 (2014).
 47. H. Kogelnik, and V. Ramaswamy, "Scaling rules for thin-film optical waveguides," *Appl. Opt.* 13, 1857–1862 (1974).
 48. Pitarke, J. M., V. M. Silkin, E. V. Chulkov, and P. M. Echenique. "Theory of surface plasmons and surface-plasmon polaritons." *Reports on progress in physics* 70, no. 1 (2006): 1.
 49. S. A. Taya, and K. Y. Elwasife, "Guided modes in a metal-clad waveguide comprising a left-handed material as a guiding layer," *Int. J. Research and Reviews in Applied Sciences* 13, 294–305 (2012).
 50. H. F. Taylor, and A. Yariv, "Guided wave optics," *Proceedings of the IEEE* 62, 1044–1060 (1974).
 51. Du, Cheng-Han, and Yih-Peng Chiou. "Ultra-Compact Directional Coupler Using Hybrid Plasmonic Waveguide with Dual Metallic Layers,"
 52. Meng, Lingyan, Tengxiang Huang, Xiang Wang, Shu Chen, Zhilin Yang, and Bin Ren. "Gold-coated AFM tips for tip-enhanced Raman spectroscopy: theoretical calculation and experimental demonstration." *Optics express* 23, no. 11 (2015): 13804-13813.
 53. Bian, Yusheng, and G. Qihuang, "Low-loss light transport at the subwavelength scale in silicon nano-slot based symmetric hybrid plasmonic waveguiding

- schemes,” *Opt. Express* 21, 23907–23920 (2013).
54. M. Toishi, D. Englund, A. Faraon, and J. Vučković, “High-brightness single photon source from a quantum dot in a directional-emission nanocavity,” *Opt. Express* 17(17) 14618-14626 (2009).
 55. Fushman, Ilya, Dirk Englund, and Jelena Vučković. "Coupling of PbS quantum dots to photonic crystal cavities at room temperature." *Applied Physics Letters* 87, no. 24 (2005): 241102.
 56. Vučković, Jelena, and Yoshihisa Yamamoto. "Photonic crystal microcavities for cavity quantum electrodynamics with a single quantum dot." *Applied Physics Letters* 82, no. 15 (2003): 2374-2376.

ABSTRACT**LOCAL FIELD ENHANCEMENT ON DEMAND BASED
ON HYBRID PLASMONIC-DIELECTRIC
DIRECTIONAL COUPLER**

by

KHOLOD ADHEM**December 2016****Advisor:** Dr. Ivan Avrutsky**Major:** Electrical Engineering**Degree:** Doctor of Philosophy

The concept of local field enhancement using conductor-gap-dielectric-substrate (CGDS) waveguide structure is proposed. The dispersion equation is derived analytically and solved numerically. The solution of the dispersion equation reveals the anti-crossing behavior of coupled modes. The optimal gap layer thickness and the coupling length of the guided modes are obtained. The mechanism of the CGDS system works as follows: Light waves are guided by conventional low-loss dielectric waveguide and, upon demand, they are transformed into a highly confined plasmonic mode with a strong local field enhancement, and get transformed back into low-loss dielectric mode. As an example, in a representative CGDS structure, the optimal plasmonic gap size is 17 nm, the local light intensity is found to be more than one order of magnitude stronger than the intensity of the dielectric mode at the film surface. The coupling length is only 2.1 μm at a wavelength of 632.8 nm. Such a local field

confinement on demand is expected to facilitate efficient light-matter interaction in integrated photonic devices while minimizing losses typical for plasmonic structures.

AUTOBIOGRAPHICAL STATEMENT

Kholod Adhem received her Bachelor of Science in Electrical Engineering from Tripoli University, Tripoli, Libya in December 2007. After finishing her Bachelors, she pursued Master of Science in Electrical Engineering and graduated from Wayne State University, Detroit, Michigan in August 2011. She then started her Ph.D. research work in Integrated Optics and Nanophotonic lab in Elcetrical Engineering at Wayne State University under the guidance of Dr. Ivan Avrutsky. She authored a manuscript in Optics Express Journal. She is a member of Tau Beta Pi, The Engineering Honor Society, and she is also a member in the Golden Key Engineering Society. She expects to graduate in December 2016.